UNIVERSITÀ
DI SIENA
1240

LPOSOMAL ENCAPSULATION OF CITICOLINE FOR OCULAR DRUG DELIVERY, AND POLYSACCHARIDE BASED HYDROGELS FOR ARTICULAR CARTILAGE TREATMENT

By

Fariba Fahmideh Mahdizadeh

Supervisor:

Prof. Agnese Magnani

Co-supervisor:

Dr. Brian Amsden

Chemistry and Pharmaceutical Sciences

Department Biotechnology, Chemistry and Pharmacy

Doctoral thesis | Siena University | 2022-2023

Abstract

Glaucoma represents a group of neurodegenerative diseases characterized by optic nerve damage and the slowly progressive death of retinal ganglion cells. Pharmaceutical treatment of glaucoma is problematic because the properties of the ocular barrier limit the penetration of ocular drugs, resulting in lower systemic bioavailability. This problem conditions frequent drug administration, which leads to the deposition of concentrated solutions on the eye, causing toxic effects and cellular damage to the eye. To overcome these drawbacks, novel drug delivery systems such as liposomes play an important role in improving the therapeutic efficacy of anti-glaucomatous drugs. In this work, liposomes were synthesized to improve various aspects, such as ocular barrier penetration, bioavailability, sustained release of the drug, targeting to the tissue, and reduction of intraocular pressure. Citicoline (CDP-choline; cytidine 5′-phosphocholine) is an important intermediate in the biosynthesis of cell membrane phospholipids, with neuroprotective and neuroenhancement properties. Citicoline was used in the treatment of retinal function and neural conduction in the visual pathways of glaucoma patients. In this study citicoline was loaded in the DOPC:CH liposomal carrier to improve its therapeutic effects. The citicoline-encapsulation efficiency, drug leakage and size analysis of various liposome systems were studied.

Cartilage injury is still a concern to humans since it does not cure on its own, and there is presently no treatment available to entirely restore cartilage function. A porous, three-dimensional network material called hydrogel, which can hold a lot of water and is insoluble in water, is frequently utilised in the medical industry and has outstanding mechanical qualities. To repair cartilage, researchers are particularly interested in the mechanical characteristics and biocompatibility of hydrogel constructed of composite materials. The features of natural extracellular matrix (ECM), good biocompatibility, and strong flexibility to adapt to irregular

cartilage defect surfaces are the key benefits of injectable hydrogels for cartilage injury. Injectable hydrogels are a promising approach for the engineering of cartilage tissue because of their inherent features. To take advantage of a combination of both chemical and physical crosslinking, freeze-thaw Poly(vinyl alcohol) (PVA) micro-particles were manufactured first and incorporated in various concentrations to chondroitin sulphate hydrogel, as a natural polysaccharide. This process produced an injectable hydrogel with a high modulus that is suitable for applications involving load-bearing soft tissues (LBST) with high moduli, such as cartilage. The effect of several parameters such as cross-linking conditions and prepolymer concentrations on the mechanical characteristics of hydrogels were studied.

List of the original publications

A. Leone, G.; Pepi, S.; Consumi, M.; Mahdizadeh, F.F.; Lamponi, S.; Magnani, A. Phosphorylated Xanthan Gum-Ag(I) Complex as Antibacterial Viscosity Enhancer for Eye Drops Formulation. *Carbohydr Polym* **2021**, *267*, doi:10.1016/j.carbpol.2021.118196.

B. Fort, A.; Landi, E.; Grasso, A. lo; Mugnaini, M.; Panzardi, E.; Vignoli, V.; Mahdizadeh, F.F.; Magnani, A. Monitoring of the Viscoelastic Behaviour of Bacterial Biofilms Exploiting an Accurate QCM System. In Proceedings of the 2022 IEEE International Symposium on Medical Measurements and Applications, MeMeA 2022 - Conference Proceedings; Institute of Electrical and Electronics Engineers Inc., 2022.

C. Bonechi, C.; Talarico Luigi, Leone, G.; Pepi, S.; Consumi, M.; Mahdizadeh, F.F.; Lamponi, S.; Magnani, A, Liposomal encapsulation of citicoline for ocular drug delivery, submitted.

Acknowledgements

First and foremost, I am extremely grateful to my primary supervisor, Prof. Agnese Magnani, for her invaluable advice, continuous support, and patience during my Ph.D. study. I would not be where I am or who I am today without your endless support.

Thank you to my co-supervisor at Queen's University, Dr. Brian Amsden, for your time and the opportunities you provided for me to improve my research and communication skills during our weekly individual meetings, and group meetings. I would also like to thank you for being such a wonderful group of people, both in and out of the lab. It has been an amazing experience working with two research groups across different continents.

I would like to thank the University of Siena for providing me with the resources to pursue graduate study. Thank you to all my lab mates at Siena University, Lorenzo, Simone, Flavia, and Luigi, for their unending support. I have so missed our coffee and lunchtime breaks together.

Thank you to all members of the Amsden lab for all your time spent discussing my research study. Ronghui, in particular, thanks for all your help, support, and friendship; you are inclusivity is appreciated by many. Hossein, I've been so pleased to have you being able to discuss ideas which have really been invaluable.

I'd like to express my gratitude to Dr. Marco Consumi and Dr. Gemma Leone, my esteemed advisors, for all the guidance, technical support, and instruction they provided me throughout my doctoral studies.

Furthermore, I value the love and encouragement of my parents. Finally, I'd like to express my gratitude to my husband who has been a constant source of support and encouragement during the challenges of academic life. I am truly thankful for having you in my life.

Table of Contents

List of Tables

List of Figures

List of Abbreviations and Symbols

AMD	Age-related macular degeneration
CH	Cholesterol
Cit	Citicoline
CS	Chondroitin sulfate
DDS	Drug Delivery Systems
DLS	Dynamic light scattering
DM	Degree of methacrylation
DMSO	Dimethyl sulfoxide
DOPC	1,2-dioleoyl-sn-glycero-3-phosphocholine
DR	Diabetic retinopathy
ECM	Extracellular matrix
EE	Encapsulation efficiency
IOP	Increased intraocular pressure
kDa	Kilodalton
LUV	Large unilamellar vesicles
MLV	Multilamellar unilamellar vesicles
MW	Molecular Wight
MWCO	Molecular weight cut off
NaOH	Sodium hydroxide
NMR	Nuclear magnetic resonance
NRU	Neutral red uptake
PBS	Phosphate Buffer Saline

PDI	Polydispersity index
POAG	Open-angle glaucoma
PVA	Poly (vinyl alcohol)
SUV	Small unilamellar vesicles
UV	Ultraviolet

Chapter 1: Literature Review

1.1 Application of Liposomes as ocular drug delivery

1.1.1 Anatomy and physiology of the posterior eye segment

The small but incredibly complicated human eye is the organ that allows for vision. The anterior and posterior segments of the eye can be classified (Figure 1). The anterior segment consists of the cornea, iris, ciliary body, aqueous humour, conjunctiva, and lens. The vitreous fluid, retina, and choroid make up the posterior segment of the eye, which is the area behind the lens [1].

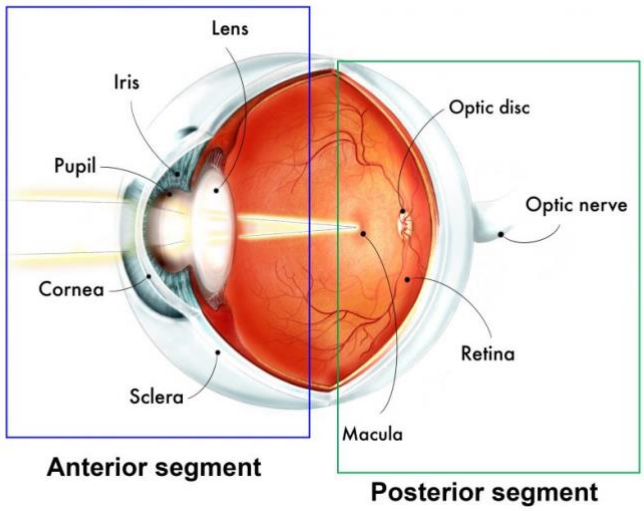

Figure 1: The human eye anatomy [2].

Vitreous Humor

A clear, colourless jelly-like material called vitreous humour is found between the lens and the retina. It occupies nearly all the eyeballs (98%) and is mostly made of water. It maintains the retina in place and aids in maintaining the shape of the eye.

Retina

The layer in the back of the eye that detects light is called the retina. It consists of various types of specialized cells that work together to create an image to see. Photoreceptors are one of these cells. They recognize light entering the eye and transform it into electrical signals, which are subsequently sent to the brain by several specific cells in the retina and the optic nerve.

The optic nerve

The eyes and brain communicate with one another via the optic nerve to create a visual image (what we see). An electrical impulse is produced when the retina's photoreceptor cells detect light, and this impulse is subsequently sent to the brain via the optic nerve.

1.1.2 Common posterior segment eye diseases

The retina is impacted by many disorders that compromise eyesight. Aging and/or underlying illnesses (including diabetes, hypertension, and atherosclerosis) are linked to many posterior segment disorders[3]. The most common conditions causing increased vision loss in ageing populations globally include age-related macular degeneration (AMD), diabetic retinopathy (DR), and glaucoma [4]. The optic nerve and ganglion cells are two of the eye conditions referred to together as glaucoma. These effects may cause varying degrees of visual loss and blindness if left unchecked. Increased intraocular pressure (IOP) continues to be the main risk factor for glaucoma development. Based on the causes of elevated intraocular pressure, glaucoma is often categorized as either open angle or angle closure (closed angle) [5]. The open-angle glaucoma is the most common type of glaucoma. In primary open-angle glaucoma (POAG), the drainage angle that leads to the trabecular meshwork looks normal, but aqueous fluid exits the eye too slowly (Figure 2). On the other hand, angle-closure glaucoma is a less common type of glaucoma where the drainage is too narrow or begins to close, impeding the normal outflow of aqueous humor. Angle-closure glaucoma can be either chronic (anatomically narrow-angle or

temporary episodes of angle closures over time) or acute (the angle narrows or closes suddenly). The term narrow-angle glaucoma often is used to describe glaucoma that occurs when the drainage angle is too small or is partially closed.

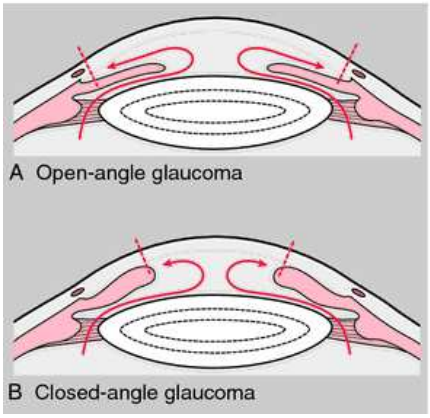

Figure 2: Glaucoma. A) in open-angle glaucoma, the obstruction occurs in the trabecular meshwork. B) in closed-angle glaucoma, the trabecular meshwork is covered by the root of the iris or adhesions between the iris and cornea [5].

1.1.3 Methods for ophthalmic drug delivery

Any ocular medication delivery system must maintain therapeutic drug concentration at the target location for long enough dosing intervals to be effective. It is necessary to understand ocular barriers in drug development since drug concentrations at target sites depend on drug penetration through the barriers. Eye drops or ointments are frequently utilized for anterior drug administration, but not for posterior drug delivery. There are a few typical methods for delivering ophthalmic drugs to the posterior region of the eye (Figure 3). By topical administration (eye drops), there are two ways to deliver medications to the posterior ocular segment: first (Route 1), the medication diffuses to the conjunctiva from the ocular surface, then passes through the sclera pore to the posterior choroid and choroidal circulation, and finally reaches the RPE layer from the choroidal vessels. The drug enters the eye via the corneal

surface, anterior aqueous chamber, lens, and vitreous body on the second (Route 2). From there, it diffuses to the inner limiting membrane before entering the retina. In the administration method medications pass through the sclera pores to the posterior choroid and choroidal circulation before reaching the RPE layer via the choroidal arteries. Subretinal injection is represented by Route 4. Direct injection of the medication into the posterior ocular segment causes it to first diffuse to the RPE layer and then to the inner retina. Intravitreal injection is the most common method of posterior ocular medication administration (Route 5 in the diagram). The medication is injected into the vitreous humour, where it diffuses in several directions before crossing the inner limiting membrane and entering the retina. The effectiveness of intravitreal injection for the transport of retinal drugs is greatly reduced because of the complexity of the three-dimensional network of collagen fibres connected by proteoglycan filaments in the vitreous body. Additionally, the drug's limited absorption and inability to penetrate the retina are caused by the vitreous humor's colloidal form. There is an internal limiting layer that serves as a barrier to stop drug penetration into the retinal cells even if the drug can reach the retina. Finally, Route 6 delivers the medicine from the systemic circulation to the RPE layer. The posterior region of the eye can occasionally be reached with oral drugs, although it can be challenging to administer an effective dose in some circumstances [6].

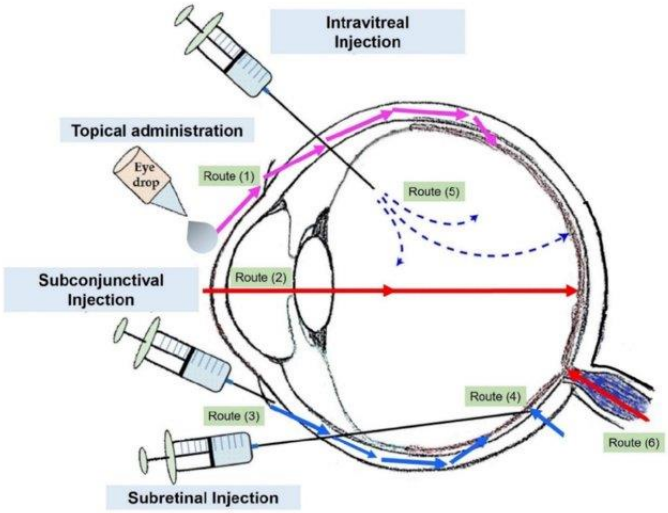

Figure 3: Ocular medication administration techniques and routes to the posterior region. Via topical administration (1 and 2) subconjunctival injection (3) subretinal injection (4) and intravitreal injection (5) to the back of the eye (5) via systemic circulation (6) The comparison of conventional and advanced topical ocular drug delivery systems [7]

Undoubtedly one of the most challenging issues facing pharmaceutical researchers is the delivery of ocular medications. Their goal is to reach and keep a therapeutic level at the action site for a considerable amount of time. Novel drug delivery techniques (Figure 4) should be developed to maintain medicine levels at the target place for a long time. Novel drug delivery systems are just entering the market and are modifications of older ones in terms of distinct delivery techniques or tools to be utilized before, during, or after administration. As new technologies are developed, existing treatments are losing their effectiveness. New drug delivery techniques enhance a drug's therapeutic effects while minimizing its negative effects by reducing drug exposure to non-target cells and enhancing the amount and durability of a drug surrounding target cells. Due to several features, such as quick yield, limited absorption, short residence time, and generally impermeable medicines, traditional administration techniques have poor ocular bioavailability (less than 1%). Up to 80% of the dose may be lost after 5 minutes of ingestion due to tears leakage.

The length of therapy may be prolonged by using viscosity enhancers, ophthalmic solutions in which the drug dissolves slowly, or ocular inserts. Ophthalmic medication delivery is ideal because it delays drug release and permits better contact with the front of the eye. Novel ocular medication administration seeks to increase drug bioavailability by facilitating trans-corneal drug penetration or extending the time of medicine retention in the eye. Eye drops and ointments are the ophthalmic medications that are most frequently readily hand. However, these preparations are quickly emptied from the ocular chamber due to tear flow and lachrymal nasal drainage. Frequent dosage is necessary since just a tiny amount is accessible for therapeutic effect. To deal with these issues, more modern pharmaceutical ophthalmic formulations have been developed over the previous three decades. In situ gels, nanoparticles, liposomes, nano-suspensions, microemulsions, iontophoresis, and ocular inserts are a few of these formulations[8].

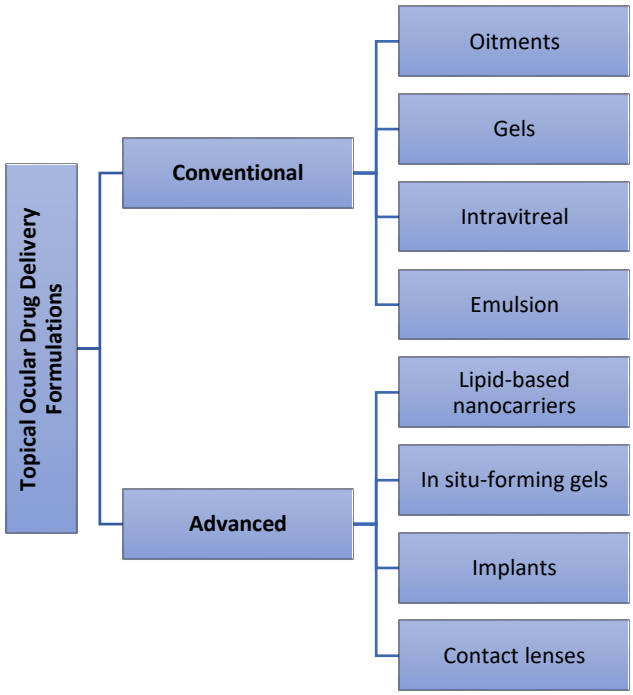

Figure 4: Conventional vs novel topical ophthalmic therapies [8].

1.1.4 Nanocarriers for the posterior segment eye diseases

The bioavailability of ocular medications may be constrained by the eyeball's intricate anatomy, which contains a variety of obstacles. Various ocular medication delivery methods have recently been developed. These consist of lipid-based nanocarriers, hydrogels, polymeric micelles, and nanosuspensions (Figure 5). As delivery systems for ocular administration, lipid-based nanocarriers such as emulsions, liposomes, niosomes, and others present some potential benefits, including increasing the bioavailability of poorly soluble drugs, providing targeted and controlled release, and minimizing side effect [9]

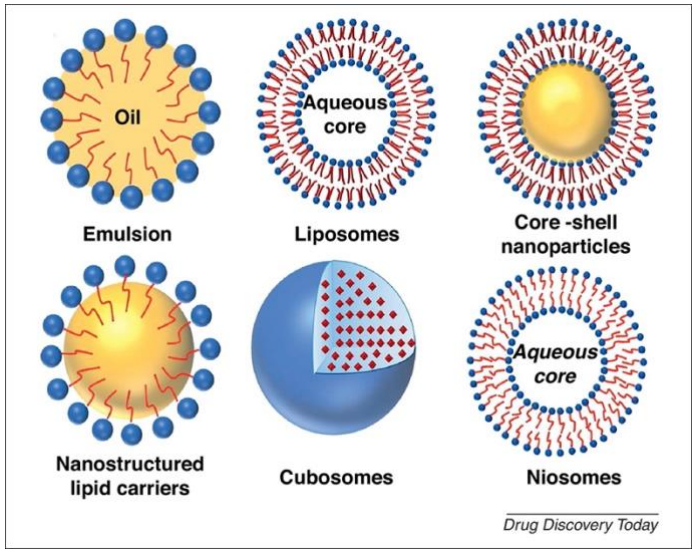

Figure 5: Schematic structures of various nanomaterial-based drug delivery systems [9].

1.1.6 Liposomes

Liposomes are biocompatible and biodegradable particles made of lipid bilayers that resemble membranes and are mostly made of phospholipids [10]. They are spherical hollow structures (vesicles) made of amphiphilic phospholipids that have both hydrophilic (aqueous compartment) and lipophilic (lipid bilayer) phases (Figure 6). Due to their biphasic structure, liposomes can encapsulate and carry both hydrophilic and lipophilic theopathic in each

compartment [11]. In the former, the compounds are incorporated in the aqueous part of the liposomes while in the latter they are incorporated in the lipid bilayers [12]. This structure turns liposomes into ideal drug carriers since hydrophilic drugs tend to be entrapped in the core, while hydrophobic ones will be entrapped within the lipid bilayers. Depending on the kind of lipid employed and the technique of manufacture, the creation of a suitable liposomal system as a carrier for a certain medicine is necessary. They are referred to as small unilamellar vesicles (SUV) or giant unilamellar vesicles, depending on their size (LUV). Multilamellar vesicles are referred to as such if there are additional bilayers (MLV) [13]. The main components of liposomes are phospholipids and cholesterol. The stability of the liposomal membrane is greatly influenced by cholesterol. It is generally known that cholesterol affects membrane strength, elasticity, fluidity, permeability, transition temperature (T_m), drug retention, phospholipid packing, and plasma stability [14]. Despite all the potential advantages such as low toxicity, biodegradability and stable drug release, there have been several apparent limitations of liposomes for ocular delivery application such as vision blurring and limited storage time [15].

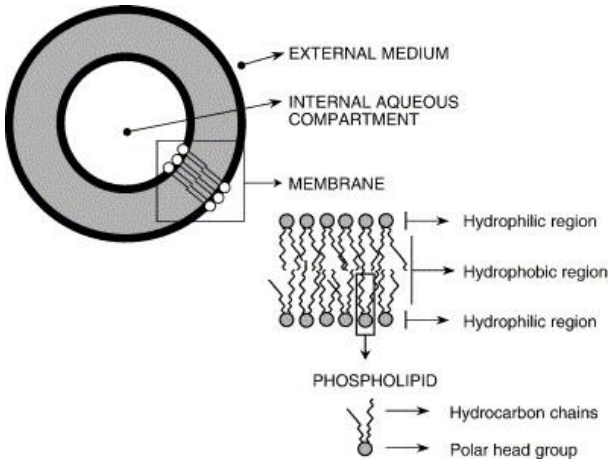

Figure 6: Basic structure and composition of unilamellar liposomes.

1.1.7 Aim (Project I)

The aim of the present research study was to encapsulate citicoline in a liposomal carrier with two different molar ratios, which is expected to improve the efficiency of drug-delivery for ophthalmic therapies. These vesicles are composed of 1,2-dioleoyl-sn-glycerol-3-phosphocholine (DOPC) and cholesterol (CH) in two different molar ratios, (1:1) and (2:1), respectively. The chemical characterization of the synthesized liposomes was evaluated in terms of particle size and surface charge, in vitro drug release and physical stability.

1.2 The effect of FT-PVA particles on the mechanical properties of hydrogel made of methacrylate chondroitin sulfate

1.2.1 Articular cartilage, anatomy, function, and mechanical properties

Osteoarthritis is a common, acute, and painful age-related condition that currently has no recognized cure. Although there are numerous unique treatments for osteoarthritis damage, it is likely that none of them will be effective in the long run if the full scope of the illness and the impact of joint biomechanics on joint tissues are not carefully considered [16]. Three different types of cartilage are found in the human body. The hyaline cartilage has an excellent ability to resist compressive forces at sites of bone articulation. The elastic cartilage, which is found on the outside of the ear, and fibrous cartilage, which is found in the menisci and intervertebral discs. Extracellular matrix (ECM) composition and structure, including cartilage fibre thickness, are characteristics of several forms of cartilage. Articular cartilage is a subset of hyaline cartilage. In relation to the objective of this thesis, the major subjects of the following paragraphs are the properties of articular cartilage. Cartilage deficiencies can be the end result of concurrent knee injuries, such as meniscal surgery or anterior crucial ligament restoration, and can be induced by trauma in adults over 60 years old. Figure 7 shows the healthy and advanced arthritis articular cartilage as well as various levels of the defects.

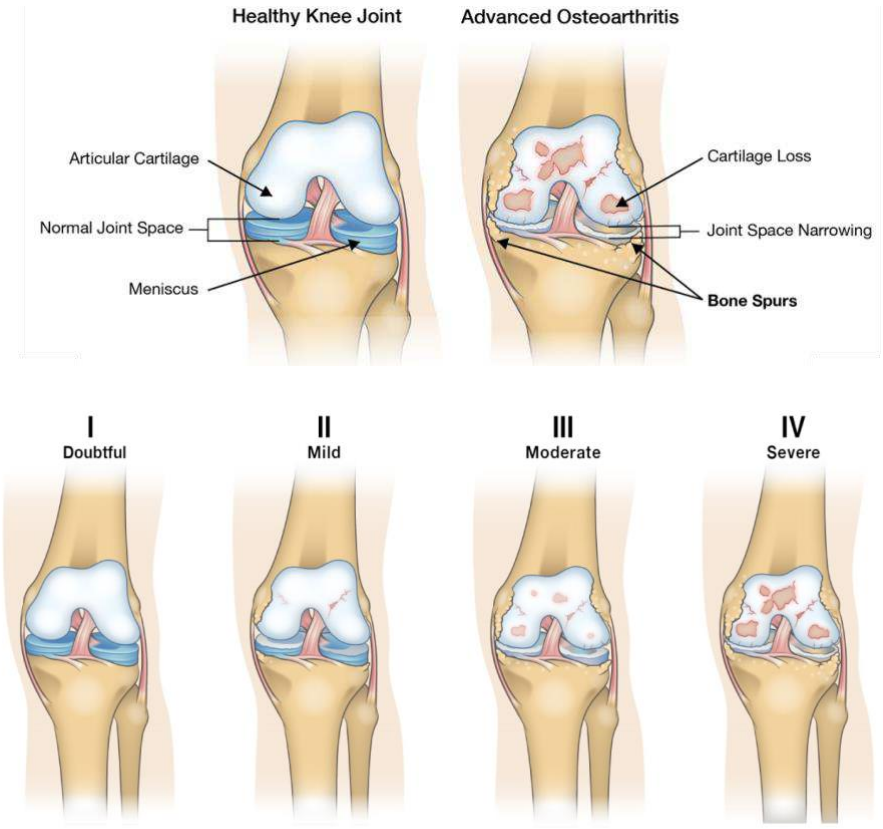

Figure 7: Different stages of cartilage defects [17] .

In contrast to the bone, hyaline articular cartilage tissue has a very low cell density, which allows for only very limited self-renewal. However, this tissue is well hydrated. This tissue has layers that differ slightly in structure such as cell density, ECM composition, and collagen fibre orientation and they determine the mechanical qualities of articular cartilage [18,19]. The mechanical properties of articular cartilage depend on the structural integrity of the constituents of the matrix composed mainly of collagen, proteoglycan (PG) and water. Since cartilage is viscoelastic, it responds to constant loads or deformations in a time-dependent manner. Viscoelasticity in articular cartilage is caused by two different types of mechanisms: flow dependent and flow independent. The frictional drag brought on by this flow and the interstitial fluid are both essential to the flow-dependent mechanism. Biphasic viscoelastic behaviour is the term used to describe the drag caused by the interstitial fluid. Macromolecular motion, more

especially the inherent viscoelastic properties of the collagen-proteoglycan matrix, is what causes the flow-independent component of viscoelasticity. As a result, a considerable portion of the overall load support is provided by the fluid pressure, which lessens the stress placed on the solid matrix. The flow-dependent mechanism depends on interstitial fluid and the frictional drag associated with this flow. Biphasic viscoelastic behaviour is the term used to describe the drag caused by the interstitial fluid. Macromolecular motion, more especially the inherent viscoelastic properties of the collagen-proteoglycan matrix, is what causes the flow-independent component of viscoelasticity. As a result, a considerable portion of the overall load support is provided by the fluid pressure, which lessens the stress placed on the solid matrix. Additionally, creep and stress-relaxation are seen in articular cartilage. When a tissue is subjected to a continual compressive stress, the tissue will deform or creep until an equilibrium value is attained. Similar to this, when cartilage is deformed and maintained at a constant strain, the stress will increase to a peak and then gradually decrease until an equilibrium value is attained [20] The material properties commonly measured include the shear modulus, relaxation modulus, Young's modulus, and instantaneous modulus (by both confined and unconfined compression). Table 1 shows the value range of some mechanical propertied of the natural articular cartilage.

Table 1: Biomechanical properties of healthy human cartilage (regardless of location).

Mechanical property	**Range of Values**	**Method**
Compression Young's modulus (MPa)	0.24–0.85 [21]	Unconfined compression
Equilibrium Relaxation Modulus (MPa)	0.1-2.0 [22]	Confined compression

1.2.2 Current treatment strategies

Surgery may be helpful and holds considerable promise for symptomatic local cartilage articular damages. Numerous articular cartilage repair and restoration techniques, such as osteochondral autograft or allograft, microfracture, cartilage transplantation, and intra-articular injections of various compounds, may help symptoms.

1.2.3 Application of CS and PVA in cartilage engineering

The most prevalent glycosaminoglycan (GAG) in the human body is chondroitin sulfate (CS), a polysaccharide that accounts for 80% of the GAGs in mature articular cartilage. CS is a D-glucuronic acid and D-N-acetylgalactosamine repeating linear sulfated GAG. It can integrate with tissue and produce an anti-inflammatory reaction. Chondroitin sulfate has wide application in most tissues from the eye to the extracellular matrix (ECM) of cartilage tissues [23]. CS-based hydrogels have been widely investigated as scaffolds for cartilage or osteochondral defects in tissue engineering. It contains a high-water content and a high charge density, which leads to mechanical weakness [24]. CS-based hydrogels have been widely investigated as scaffolds for cartilage or osteochondral defects in tissue engineering. The strength of these natural hydrogels can be increased by making the polymer matrix denser if required, using chemical cross-linking, or through chemical modifications. On the other hand, synthetic polymers with high mechanical strength show low cell affinity due to hydrophobicity and lack of cell recognition sites. Accordingly, the combination of both natural and synthetic biopolymers is widely used in cartilage engineering [25]. This combination can promote biodegradability, cell attachment, and hydrophilicity properties [26]. Poly (vinyl alcohol) (PVA) as a synthetic and water-soluble polymer has been widely investigated for biomedical applications. It has good biocompatibility, mechanical strength and toughness, low friction, and high lubricity. This polymer can create concentrated zones of hydrogen bonds between -

OH groups of its chains (crystalline zones) when frozen [27]. However, it does not efficiently support cell adhesion on its surface owing to the hydrophilicity provided by the hydroxyl groups (OH) along its backbone [28]. Based on the potential of PVA, it is hypothesized that the incorporation of PVA in CS hydrogels like a filler may enhance the mechanical strength of the hydrogels.

1.2.4 Aim (Project II)

The objective of this study is to enhance the mechanical properties of in-situ forming biopolymer-based hydrogels applied for articular cartilage treatment. To reach this objective, CS was functionalized with methacrylate groups and combined with freeze-thaw PVA (FT-PVA) particles. Following photo-crosslinking, a hybrid CS-PVA hydrogel was formed and subsequently mechanically analyzed as well as its water and sol content were measured. Matrix stiffness was controlled by tuning the concentration of FT-PVA particles. The matrix so formed was compared with a control hydrogel made with and without FT-PVA particles.

Chapter 2: Liposomal encapsulation of citicoline for ocular drug delivery

2.1 Introduction

The central nervous system (CNS) includes the retina, or the neural section, of the eye. Six distinct neural kinds make up its neuronal component. A set of eye conditions known as optic neuropathies includes glaucoma, anterior ischemic optic neuropathy, and retinal ischemia. The cells most frequently impacted in optic neuropathies are retinal ganglion cells (RGCs), one of the six neurons in the retina. The retina's output cells, or RGCs, provide visual signals to the brain through virtual targets. The most prevalent optic neuropathy, glaucoma, is a complex group of progressively degenerative visual neuropathies that can result in blindness [29]. Glaucoma is defined by the death or degeneration of RGCs. It is a neurodegenerative condition that affects the brain's visual and ocular structures [30]. There are significant similarities between this neurodegenerative eye illness and neurodegenerative brain disease.

Because it can harm the retina's optic nerve, intraocular pressure (IOP) is regarded as the most significant and the only modifiable risk factor for glaucoma. Although high IOP can kill RGCs, the harm to the optic nerve may persist even after IOP has been reduced. The secondary degradation of nearby neuronal cells in the extracellular environment is caused by the injured RGCs via the trans-synaptic process, which starts at an early stage of glaucoma and is not just a result of the high IOP factor [31]. IOP is not the only risk factor contributing to the degeneration of RGCs. In order to cause RGC degeneration that results in optic neuropathy, a number of pathogenic events may take place, such as decreased microcirculation, ischemia/reperfusion injury, oxidative stress, and a lack of neurotrophic growth factor [32]. RGCs have been protected and visual function has been recovered using a variety of directed and undirected procedures. RGC neuroprotection is a technique that uses chemicals, such citicoline, to keep RGCs safe [29]. The endogenous chemical citicoline (cytidine-5'-

diphosphocholine) (Figure 9) is necessary for the synthesis of acetylcholine and membrane phospholipids as well as for elevating neurotransmitter levels in the central nervous system. The neuroprotective properties of citicoline in glaucoma have been defined, in particular its induces antiapoptotic effects, increases retinal dopamine levels, and counteracts thinning of the retinal nerve fiber layer [33]. Citicoline administered intramuscularly has enhanced RGC function, neuronal conduction post-retinal, and glaucomatous visual abnormalities [34,35]. This hydrophilic, naturally occurring, endogenous substance has had a major impact on glaucoma, Parkinson's, Alzheimer's, and brain ischemia, among other systemic neurodegenerative diseases [36]. The central nervous system uses this nutrient to generate membrane phospholipids [37]. Instead of oral medicines with a low dosage and significant adverse effects, ocular administration is a difficult topic that has drawn many scientists working on it [38]. Topical ophthalmic medications can be found in a variety of formulations, including liquid, solid, and semisolid. However, other drug delivery methods, such as multicompartment ophthalmic systems, have certain benefits [39]. One of the drug carriers in the category of multicompartment drug forms are the liposomes. In recent years, liposomal ophthalmic formulations have become popular for use in drug delivery systems. Due to their biodegradability and lack of toxicity, liposomes have several benefits over alternative ocular delivery technologies. Additionally, their use in ophthalmic drug forms improves the bioavailability of formulations with loaded molecules against the enzymes found on the corneal epithelium's surface, in contrast to traditional ophthalmic formulations like solutions, which lack bioavailability properties. Unilamellar and multilamellar vesicles (ULV and MLV), with sizes ranging from 10 nm to 1 μm, and bilayers of lipid vesicles, make up liposome vesicles. They have been widely used as carriers for delivering bioactive substances because they resemble the lipid membrane of living cells [38,40]. Drug-loaded liposomes have been used to treat a variety of ocular illnesses in both the anterior and posterior segments over the past ten

years. They are made primarily of phospholipids and other components, such as cholesterol, and are generated in aqueous solutions [41]. They are regarded as lipid-type molecules, which are crucial for the structural integrity of cell membranes. Cholesterol is a rigid and almost planar molecule [42]. Additionally, it improves the bilayer membrane's fluidity and lessens molecular leakage that involves water [43]. An inner aqueous compartment of vesicles is surrounded by lipids. They can encapsulate both hydrophilic and hydrophobic active compounds thanks to this property. The interior aqueous section is filled with capsules that contain water-soluble medications like citicoline. Reverse-phase injection, organic solvent injection, thin-film hydration, and dehydration-rehydration are some of the different liposome preparation techniques. The thin-film hydration technique is thought to be the most popular one [44]. Drug loading can be attained either passively (i.e., the drug is encapsulated during liposome formation) or actively (i.e., after liposome formation). Passive encapsulation of water-soluble drugs depends on the ability of liposomes to trap aqueous buffer containing a dissolved drug during vesicle formation. The aim of the present research study was to encapsulate citicoline in a liposomal carrier with two different molar ratios, which is expected to improve the efficiency of drug-delivery for ophthalmic therapies. These vesicles are composed of 1,2-dioleoyl-sn-glycerol-3-phosphocholine (DOPC) and cholesterol (CH) in two different molar ratios, (1:1) and (2:1). The chemical characterization of the synthesized liposomes was evaluated in terms of particle size and surface charge, in vitro drug release and physical stability. The physicochemical properties of liposomes were studied to evaluate the behaviour of citicoline in the presence of bilayers and to highlight its ability to deliver drugs. In particular, conformational properties were determined by nuclear magnetic resonance (NMR), attenuated total reflection fourier transform infrared spectroscopy (ATR–FTIR) and Time-of-flight secondary ion mass spectrometry (ToF-SIMS) experiments and biological properties by in vitro drug release and cell cultures. Stability studies were also performed on

all liposomal preparations to evaluate their storability as a pharmaceutical form. These studies are important to evaluate the potential use of citicoline in liposomes for ophthalmic applications, with the aim of improving patient compliance and avoiding the administration of too many eye drops.

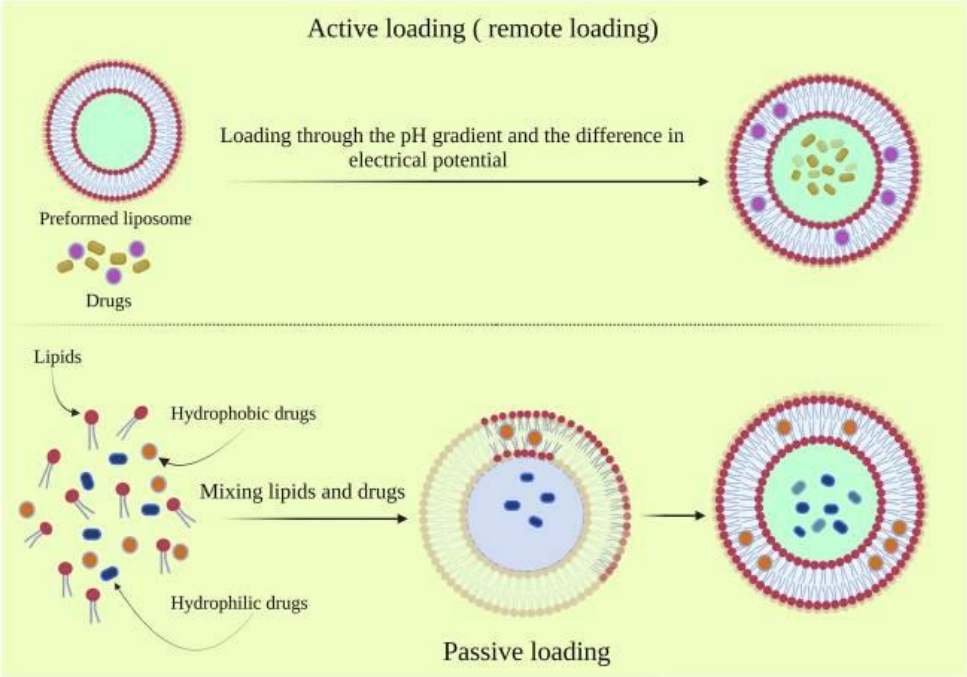

Figure 8: The active and passive drug loading on the liposomes [12].

2.1.1 Drug profile

In terms of chemistry, citicoline is Cytidine 5'-trihydrogen diphosphate p'-[2-trimethylammonio] ester inner salt, and it is a complex organic compound that serves as an intermediary in the manufacture of phosphatidylcholine (Figure 9). The CDP-choline biomolecule is a member of the class of "nucleotides" in living systems, which are crucial for cellular metabolism [45]. The central nervous system (CNS) is where citicoline is incorporated into the membrane and microsomal phospholipid fraction after being easily absorbed in the GI tract and broadly dispersed throughout the body. In addition to increasing brain metabolism

and altering the levels of various neurotransmitters, citicoline also triggers the creation of structural phospholipids in neuronal membranes [46]. Particularly, Citicoline enters the cells and gets converted into its two components: cytidine and choline. (Citicoline is a Source of Choline, Cytidine, and Phosphate). Choline, as a precursor, undergoes a series of reactions to form phosphatidylcholine (PC), which is a major phospholipid in cell membranes. This process involves the attachment of choline to a glycerol backbone and subsequent addition of fatty acids. Cytidine is converted to cytidine triphosphate (CTP), a nucleotide involved in various cellular processes. CTP then participates in a reaction with diacylglycerol (DAG) to form cytidine diphosphate-diacylglycerol (CDP-DAG). CDP-DAG serves as an activated intermediate that can donate a phosphatidyl group to other molecules. It reacts with phosphatidic acid (PA), forming phosphatidylcholine (PC), which is a key component of cell membranes. Citicoline has also several advantageous effects in CNS damage models as well as cognitive boosting, neuroprotective, and neurological illnesses of the brain that include stroke, brain, trauma, Alzheimer's, and Parkinson's disease [47].

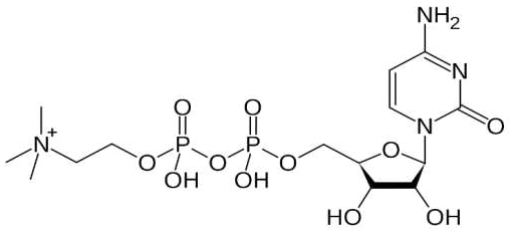

Figure 9: Chemical structure of citicoline.

Molecular Formula: $C_{14}H_{25}N_4NaO_{11}P_2 \cdot 2H_2O$

Molecular Weight: 546.34 g/mol.

IUPAC name: P′-[2-(Trimethylammonio)ethyl]ester cytidine 5′-(trihydrogen diphosphate) inner salt monosodium

Other name: Cytidine 5'-diphosphocholine sodium diphosphate salt dihydrate

Solubility: H_2O: 100 mg/ml

Appearance: White solid

Storage temperature: -20 ˚C

Solubility: In water 100 mg/ml, in PBS 10 mg/ml

Company: Sigma Aldrich

Melting point: 259-268

2.1.2 Structural Components Present in Liposomes

Phospholipids

The lipids that are most frequently utilized to create liposomes are biodegradable and biocompatible phospholipids. As they form stable bilayers in aqueous solutions, lipids with a cylindrical molecular structure, such as phosphatidylcholine, phosphatidylserine, phosphatidylglycerol, and sphingomyelin, are typically utilized for liposome formulations. Because of their suitable stability and resistance to fluctuations in pH or salt concentrations in the product or/and biological environment, phosphatidylcholines are the most employed of these lipids [48]. In terms of the structure, the phospholipids have consisted of two fatty acid chains and a polar head that has the electric charge that is attracted to the water (hydrophilic). Phospholipids are esters of glycerol. Two positions of the glycerol backbone are esterified with fatty acids of varying length and degree of saturation. Depending on the structure of this alcohol, different types of phospholipids comprise. 1,2-dioleoyl-sn-glycero-3-phosphocholine (DOPC) as one type of phospholipids is amphipathic zwitterionic phospholipids (Figure 10). They are crucial for building the protective barrier, or membrane, around your body's cells. The lipid bilayer acts as a barrier to the passage of molecules and ions into and out of the cell. The three major kinds of membrane lipids are phospho-lipids, glycolipids, and cholesterol.

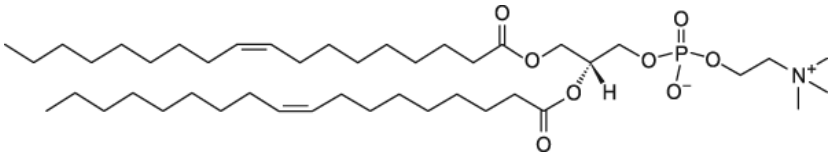

Figure 10: Chemical structure of 1,2-dioleoyl-sn-glycero-3-phosphocholine (DOPC).

Cholesterol

Cholesterol is a lipid-containing steroidal ring with an attached hydroxyl group (Figure 11). Every cell in our bodies contains cholesterol. It plays a crucial role in cell structure and the synthesis of hormones, vitamin D, and digestive enzymes. Because cholesterol is a relatively planar steroid that modifies the rigidity of lipids, it is typically combined with phospholipids in a ratio of 20–30% during the preparation of liposomes. This increases the encapsulation efficiency of liposomes by making the phospholipids stiffer and more oriented (Figure 12)[49]. The presence of cholesterol in the lipid membrane also aids in improving the stability of liposomes and lowering membrane permeability. The characteristics of cholesterol cause the bilayer's fluidity or micro-viscosity to change [50].

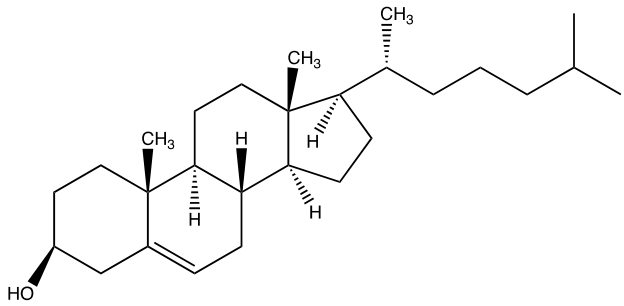

Figure 11: Chemical structure of Cholesterol.

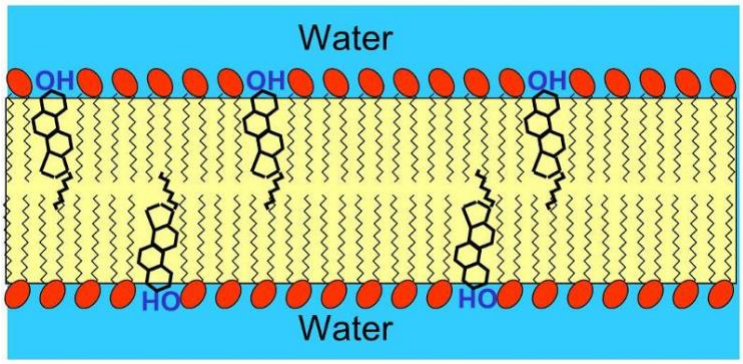

Figure 12: Schematic of presence of cholesterol in lipid bilayer [50].

2.2 Experimental

2.2.1 Materials and reagents

1,2-dioleoyl-sn-glycero-3-phosphocholine (DOPC) was purchased from Avanti Polar Lipids. Cholesterol (CH) was obtained from Sigma Aldrich (St. Louis, MO, U.S). Cytidine 5′-diphosphocholine sodium salt dihydrate (Citicoline sodium) was purchased from Sigma Aldrich. Chloroform, dialysis tubing cellulose membrane (14 kDa) and other materials were all received from Sigma Aldrich (St. Louis, MO, U.S).

2.2.2 DOPC/cholesterol liposome preparation (Plain and drug-loaded liposome)

DOPC: CH (1:1 and 2:1 molar ratio) liposomes were prepared by the film-hydration method. Briefly, lipid was mixed with chloroform (4.0×10^{-4} M) and evaporated using a nitrogen purge gas. The thin lipid film was dried in an oven at 50 ˚C for 15h to ensure that the organic solvent has been removed from the film. The lipids were hydrated by phosphate buffer saline (PBS) and loaded with drug compounds dissolved in PBS and then placed in a water bath at a temperature of 50 ˚C. The liposomes were vortexed and subjected to 10 cycles of freeze-thaw (−196 ˚C for 2 min, 50 ˚C for 5 min), as depicted in Figure 13. Freeze-thaw cycling is an important processing step in the preparation of liposomes that leads to the encapsulation of drug molecules [51]. Freeze-fracture electron microscopy revealed that these unsaturated lipids form unilamellar vesicles after 10 cycles of freeze-thawing [52]. The liposomes were then extruded with 27 times through 100 nm polycarbonate membranes (Avastin, Ottawa, CA). The solutions were then stored in the fridge. For all samples, the final lipid concentration was 10^{-2} M. According to the preceding description, drug-loaded liposomes were made. The aqueous phase received the hydrophilic medication (Cit

solution, 5.4 mg/ml in PBS). The dialysis tubing's cellulose membrane separated free, unentrapped medication molecules from one another (MWCO 14 kDa; Sigma-Aldrich Chemie GmbH PO, Taufkirchen, Germany). Table 2 shows the compositions of liposomes and the molar ratios between the phospholipids and citicoline.

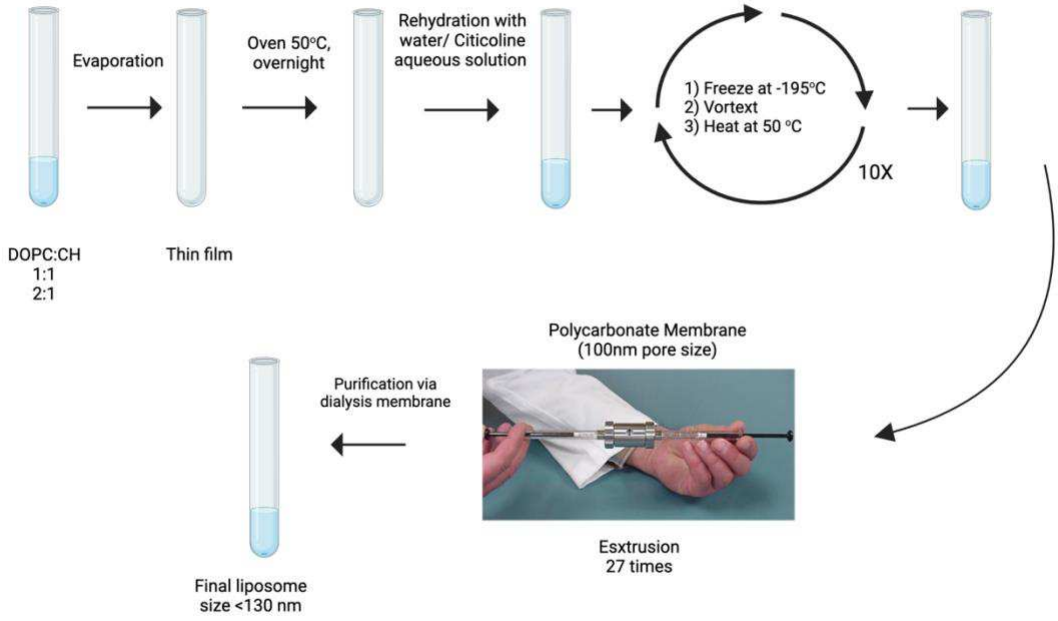

Figure 13: Representation of liposome production and encapsulation of the drug in liposome by lipid hydration followed by vortex and freezing-thaw method. Created with BioRender.com.

Table 2: Characteristics of DOPC: CH (zwitterionic) liposomes.

Sample No.	Lipid composition	Molar ratio	Initial Citicoline concentration (M)
1.	DOPC:CH	1:1	0
2.	DOPC:CH	2:1	0
3.	DOPC:CH, Cit	1:1, 1	10^{-2}
4.	DOPC:CH, Cit	2:1, 1	10^{-2}

Sample formulations:

1. DOPC:CH, 1:1
   4.10^{-2} M DOPC, in V= 125 ul chloroform => 5.10^{-6} mol DOPC
   4.10^{-2} M CH, in V= 125 ul chloroform => 5.10^{-6} mol CH
   The total used lipids: 10^{-5} mol

2. DOPC:CH, 2:1
   4.10^{-2} M DOPC, in V= 167.5 ul chloroform => $6.7.10^{-6}$ mol DOPC
   4.10^{-2} M CH, in V= 82.5 ul chloroform => $3.3.10^{-6}$ mol CH
   The total used lipids: 10^{-5} mol

3. DOPC:CH, Citicoline 1:1, 1
   4.10^{-2} M DOPC, in V= 125 ul chloroform => 5.10^{-6} mol DOPC
   4.10^{-2} M CH, in V= 125 ul chloroform => 5.10^{-6} mol CH
   The total used lipids: 10^{-5} mol

4. DOPC:CH, Citicoline 2:1, 1
   4.10^{-2} M DOPC, in V= 167.5 ul chloroform => $6.7.10^{-6}$ mol DOPC
   4.10^{-2} M CH, in V= 82.5 ul chloroform => $3.3.10^{-6}$ mol CH

   The total used lipids: 10^{-5} mol

2.3 Liposome characterization

2.3.1 Determination of Encapsulation Efficiency

The encapsulation efficiency of the loaded liposomes was measured by quantification of un-encapsulated molecules considering the initially used quantities and was detected by UV-visible spectrophotometer (Lambda 25 UV/VIS Spectrophotometer, a product of PerkinElmer Inc. spectrophotometer, in a 1cm quartz cuvette) at 272nm. Citicoline is a molecule that contains conjugated double bonds, which give it a characteristic absorption in the ultraviolet (UV) region of the electromagnetic spectrum. The absorption maximum of citicoline at 272 nm is due to the π-π* transition of the conjugated system. This transition involves the excitation of an electron from the highest occupied molecular orbital (HOMO) to the lowest unoccupied molecular orbital (LUMO) of the molecule, resulting in the absorption of the UV light. The conjugated system of citicoline is also responsible for its yellow colour, which is more intense in concentrated solutions due to increased light absorption. The free citicoline was separated from the capsuled liposomes in two subsequent steps. First, the absolute free citicoline was separated by a dialysis membrane bag in PBS for 1h agitation on a shaker and the detected values were recorded (x_1). Then to purify it from the rest of the unentrapped citicoline which was not capsulated into the liposome but still have a weak interaction with them, they were subjected to centrifugation. Briefly, 200 μL capsulated liposome aliquot was placed in Amicon centrifuged tubes, then 800 μL PBS was added to the tube and was centrifuged for 1 h at 5500 rpm by refrigerated centrifuge at 277 K (Thermo Scientific SL 16R). Then, the pellet was washed with 1ml PBS and recentrifuged for 1h. The quantity of free citicoline molecule detected in this step was recorded (x_2). The summation of x_1

and x_2 was corresponded for the total free citicoline ($C_f = x_1 + x_2$) which were calculated using the standard curve of citicoline in PBS using in equation 1.

$$EE\%: \frac{(Ci - Cf)}{Ci} \times 100 \qquad (1)$$

C_i is the concentration of the initial Cit solution added, and C_f ($x_1 + x_2$) is the quantity of detected free active molecule.

2.3.2 Size and surface charge of liposomes

The dynamic light scattering (DLS) technique was used to assess the physicochemical properties of liposomes in terms of size distribution and ζ-potential. Using DLS and the Zetasizer Nano ZS90 apparatus (Malvern, UK), equipped with a He/Ne laser of 633 nm wavelength, the analysis was conducted at pH 7.4 (PBS buffer) and 25 ˚C.

2.3.3 Nuclear Magnetic Resonance experiments (NMR)

A Bruker DRX-600 Avance spectrometer set to 600.13 MHz for 1H and outfitted with an XYZ gradient unit was used for the NMR investigations. On Silicon Graphics workstations, Bruker XWinNMR software (version 2.5) and NMRPipe software were used to process the spectra. Every sample was prepared in D_2O.

2.3.4 Standard curve of Citicoline

A double beam UV spectrophotometer has been used to create a simple, quick, accurate, precise, and affordable approach for the measurement of citicoline. A 1cm quartz cuvette was used for the ultraviolet spectrophotometric examination on a Lambda 25 UV/VIS Spectrophotometer made by

PerkinElmer Inc. The tests were made against PBS and the absorbance were measured at a wavelength of 272 nm. The standard curve for each drug release was established using the Beer–Lambert equation in the concentration range of 40-130 µg/ml with correlation coefficient (R^2) 0.9985 (Figure 14), which correlates the extinction coefficient (ε) of a substance with the absorbance (A) that was determined using equation 2.

$$A = \varepsilon.c.b \qquad (2)$$

where: ε is extinction coefficient; *c* is concentration of solution (mol/L); *b* is thickness (cm).

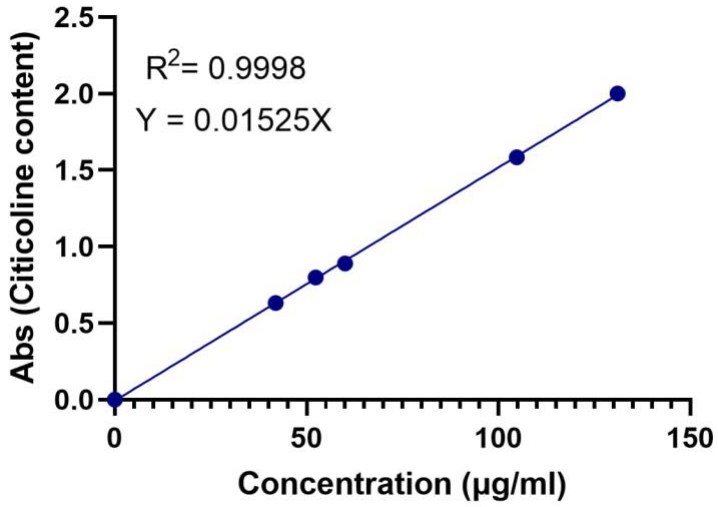

Figure 14: Calibration curve of citicoline at 272 nm in PBS.

2.3.4 In vitro drug-release profile in the eye simulation physiological fluid

In vitro release tests of liposomes loaded with citicoline were conducted utilizing a dialysis tube (MWCO 14k Da). To make sure the dialysis tube was moist and sealed, it was presoaked in eye physiological fluid obtained by emulsion oil/water [53]. Loaded liposomes (equivalent to about 54 mg/ml citicoline) were first purified against eye physiological fluid for 1h then dispersed in 0.5

mL of eye physiological fluid was placed in the dialysis bag to be released over time. Citicoline solution as a control was tested along with the liposomal dispersions. Two ends of the dialysis sac were tightly tied. The sac was hung inside a container with so that the portion of the dialysis sac with the formulation dipped into the solution. It was then submerged in 50 mL of eye physiological fluid. A shaker (IKA KS 130 basic) was used to gently shake the release medium and the liposome suspension in the dialysis tube at a rate of Mot 160/min at room temperature. At regular intervals, three aliquot samples of the release medium were taken out for detection measurements and put back into the original container. The content of citicoline in control and loaded liposomes were identified by reading the absorbance values at 272 nm by a 1cm quarts cell in a Lambda 25 UV/VIS Spectrophotometer (PerkinElmer Inc.).

2.3.5 ToF-SIMS Measurements

A TRIFT III (Phi Electronics, Chanhassen, USA) mass spectrometer time-of-flight secondary ion mass spectrometer (ToF-SIMS) equipped with a 22 keV Au+ primary ion beam gun with a beam current of 600pA at an incidence angle of 45° was used to collect a series of mass spectra. The samples were dried overnight in a conditioning pre-chamber (vacuum value of 10^{-4} Pa) and then moved to the analyzing chamber (vacuum value to 10^{-8} Pa). The scanning area of secondary ions was 100 μm × 100 μm. Selected peaks were used to calibrate positive and negative ions spectra in the low mass region: positive CH_3^+ (15.023 m/z), $C_2H_3^+$ (27.023 m/z), $C_2H_5^+$ (41.039 m/z).

2.3.6 ATR-FTIR analysis: Study of drug molecule interaction with phospholipid liposomes

Attenuated Total Reflection Fourier transform infrared spectroscopy (ATR- FTIR) was used to assess the interactions between citicoline water-soluble molecules and the lipid membranes. A

Nicolet IS50 FTIR spectrophotometer (Thermo Nicolet Corp., Madison, WI, USA) fitted with a single reflection germanium ATR crystal was used to record ATR-FTIR spectra (Pike 16154, Pike Technologies). For the collecting and modification of spectra, OMNIC software (OMNIC software system Version 9.8 Thermo Nicolet) was used. Each spectrum was averaged over 64 scans at a resolution of 4 cm^{-1} spanning the range of 4000-750 cm^{-1} in an inert atmosphere.

2.3.7 Biological studies: Mouse fibroblast cells

In vitro cytotoxicity was evaluated with NIH_3T_3 fibroblasts using the neutral red uptake (NRU) viability assay. NIH_3T_3 fibroblasts (for both controls and samples) were first planted in 24-well plates. To assess the cytotoxic effects of the system on NIH_3T_3 fibroblasts, cells were kept at 37 °C in a humid environment for 24 hours in contact with samples at various concentrations. To evaluate the in vitro cytotoxicity of liposomes a series of three concentrations ((v/v): 0.1, 1, 5) of the compounds were used in a multiwell as prepared in Table 3. All samples were tested with three replications and the control was the media without liposomes.

Table 3: A schematic of preparation of liposomes for cytotoxicity test with Mouse fibroblast cells in 24 well culture plates. (DOPC: CH), Cit), DOPC is the molar ratio of 1,2-dioleoyl-sn-glycero-3-phosphocholine, CH is the molar ratio of cholesterol, and Cit is the molar ratio of cholesterol, and Cit is the molar ratio of citicoline.

Media + 0.1 v/v (1:1), 1)	Media + 0.1 v/v ((1:1), 1)	Media + 0.1 v/v ((1:1), 1)	Media + 1 v/v ((1:1), 1)	Media + 1 v/v ((1:1), 1)	Media + 1 v/v (1:1), 1)
Media + 5 v/v (1:1), 1)	Media + 5 v/v (1:1), 1)	Media + 5 v/v (1:1), 1)	Control	Control	Control
Media + 0.5 v/v (2:1), 1)	Media + 0.5 v/v (2:1), 1)	Media + 0.5 v/v (2:1), 1)	Media + 1 v/v ((2:1), 1)	Media + 1 v/v (2:1), 1)	Media + 1 v/v (2:1), 1)
Media + 5 v/v (2:1), 1)	Media + 5 v/v (2:1), 1)	Media + 5 v/v (2:1), 1)	Control	Control	Control

Briefly, the cells were placed at the bottom of the multiwall then the media covered the cells. The observed alive cells under microscope were white. After the addition of the liposomes, they were shacked with shaker and stored in incubator at 36 ˚C with 3% CO_2 for 24h. Then the red colored stain was added to the samples, and the interaction of the liposome with cells were analyzed; the observed, red-stained cells after 24h under the microscope corresponded for the alive cells.

2.4 Results and Discussion

2.4.1 Synthesis of liposomes and drug-loaded liposomes

Zwitterionic DOPC/CH liposomes (plain and drug-loaded) were obtained by the film hydration method described in the experimental section. They were obtained with two different DOPC/CH ratios to investigate the influence of composition on their performance as nanocarriers for the

delivery of citicoline. For liposome composition and characteristics refers to Table 2 and the sample formulations described in the experimental section.

2.4.2 ζ-Potential and liposome size distribution

The size and size distribution of liposomes play an essential role in controlling the pharmacokinetics of liposomal drug formulations [54]. The results are shown in Table 4 and the corresponding distribution sizes for the DOPC:CH liposomes were reported in Figure 15 and Figure 16, measured by DLS. Saturated phosphatidylcholines are neutral zwitterionic molecules. Particle size and zeta potential of liposomes are important parameters that should be considered during the preparation of liposomes as drug delivery systems [55]. The DLS results showed that the mean particle size of plain liposomes, DOPC: CH (1:1) and DOPC:CH (2:1), were 118 ± 1 and 105 ± 3 nm, respectively. The binding of citicoline to liposomes as well as their nanoencapsulation, increased the particle sizes, indicating an increase in the hydrodynamic diameter of liposomes due to the presence of a hydrophilic molecule in the system [56]. Moreover, the size of liposomes did not vary as a function of lipid composition (or molar ratio between lipids). Cholesterol affects both the fluidity/permeability and the organization (phase and domain formation) of phospholipid bilayers [57]. In addition, the size of liposomes is the most important factor for targeting. Larger liposomes are mostly taken up by phagocytes, whereas small liposomes (<200 nm) can easily penetrate tumor tissue because of increased permeability and retention (EPR). According to this effect, small particles (<400 nm) can cross the walls of abnormal and newly formed leaky blood vessels and remain in tumour tissue [58]. Zeta potential is a key parameter that is widely used to predict the stability of suspensions. The ζ-potential of the plain liposomes was near neutrality. As the table illustrates, they showed a slight negative zeta potential charge that can be due to the preferential absorption

of H_2O ions from the water environment or to the outward exposure of phosphate groups. These values suggest that the vesicles are not more storable in solution: the aggregation or flocculation processes are many probably in solution. The greater the absolute value of zeta potential, the more stable suspension is formed [59]. DOPC: CH, Cit (1:1),1 and DOPC: CH, Cit (1:1),2 exhibited a zeta potential close to zero, -2.2 and -1.8 mV, respectively. The insertion of citicoline not modifies the structural properties of the phospholipid bilayers. The polydispersity index (PDI) is a measure of the width of unimodal size distributions [60]. Particle size of liposomes affects the drug-delivery process. In fact, small polydispersity indices of the prepared liposomes indicate good dispersion homogeneity (<0.2), suggesting that all liposomes are relatively monodisperse [61].

Table 4: Physicochemical characterization of free and drug-loaded liposomes.

Composition	Molar ratio	Initial Citicoline concentration (M)	Mean diameter (nm)	PDI	Zp (ζ) (mv)
DOPC: CH	1:1	0	118 ± 1	0.19	-4.7 ± 1
DOPC: CH	2:1	0	105 ± 3	0.19	-3.2 ± 1
DOPC: CH, Cit	(1:1), 1	10^{-2}	129 ± 0	0.19	-2.2 ± 0
DOPC: CH, Cit	(2:1), 1	10^{-2}	127 ± 2	0.20	-1.8 ± 0

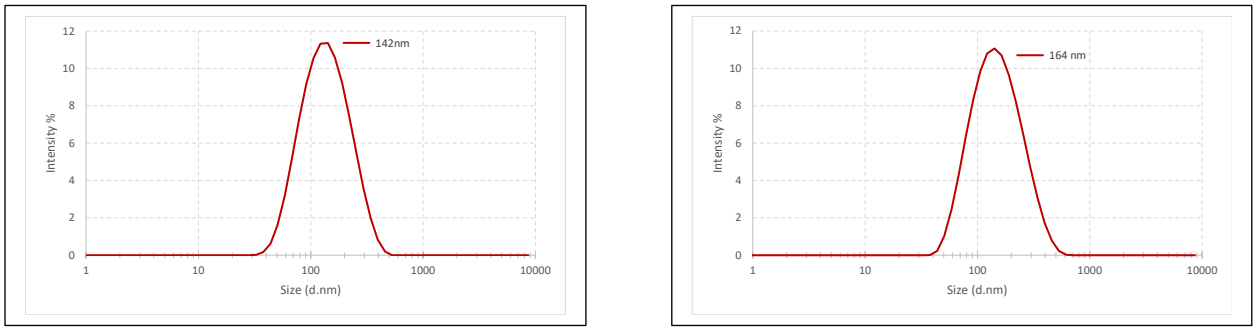

Figure 15: The size distribution of DOPC: CH (1:1) (left); DOPC: CH, Cit (1:1),1 (right).

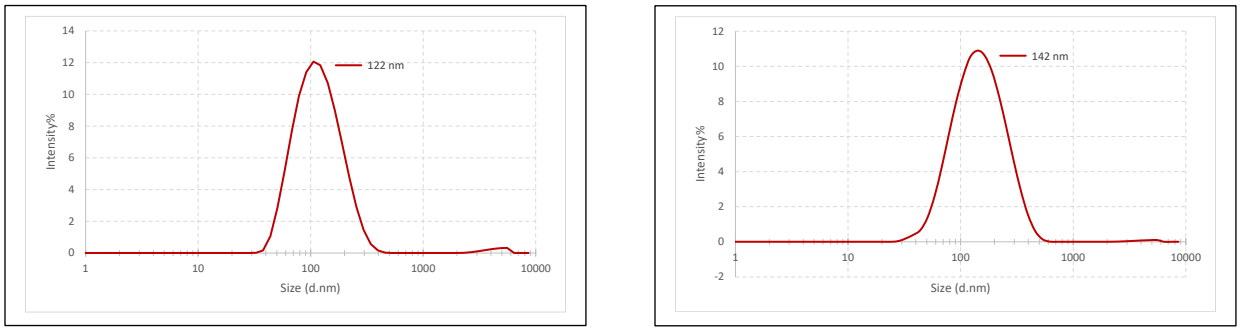

Figure 16: The size distribution of DOPC: CH (2:1) (left); DOPC: CH, Cit (2:1),1 (right).

The DLS experiments show that the citicoline insertion in the zwitterionic liposome did not modify the physical-chemistry properties of plain vesicles.

2.4.3 Determination of encapsulation efficiency

Entrapment efficiency is a critical parameter to measure the quality of liposomes, which refers to the ratio of drugs entrapped in the liposomes to the total drugs added. In addition, the key to assessing entrapment efficiency is to isolate the free (unencapsulated) drugs after the structure of the liposomes has been destroyed. The calculated encapsulation efficiency of each formulation was reported in Table 5Table 5: Encapsulation efficiency of liposomes. In this study, the free molecules were separated using a dialysis membrane and were detected by UV spectrophotometer at 272 nm and 298 K. The encapsulation efficiency of both formulations was calculated by the equation (1).

The EE % for the two liposome formulations are very high. DOPC:CH, Cit (1:1), 1 and DOPC:CH, Cit (2:1), 1 showed EE % of 40% and 47%, respectively. The zwitterionic liposomes are good systems for the encapsulation of a hydrophilic drug such as citicoline and the experimental synthesis procedure was correct to maximize this parameter.

Table 5: Encapsulation efficiency of liposomes.

Liposome	Molar ratio	Initial drug concentration (M)	Encapsulation Efficiency ± SD (%)
DOPC:CH, Cit	(1:1), 1	10^{-2}	40 ± 11
DOPC:C, Cit	(2:1), 1	10^{-2}	47 ± 11

2.4.4 Release of citicoline versus time in the eye simulation physiological fluid

Figure 17 shows the detected free citicoline at 272 nm detected by a spectrophotometer which reached its full release in 6 h of separation by dialysis membrane (MWCO 14Kda) for both the liposome formulations (1:1),1 and (2:1),1. This experiment was recorded at room temperature, and samples were shaken with a shaker during this period. The experimental results show that the formulation DOPC: CH, Cit (1:1),1 reaches a plateau more rapidly than the formulation DOPC: CH, Cit (2:1),1. Cholesterol concentration affects the release process of citicoline in physiological fluid. In particular, higher cholesterol concentrations accelerates the release of the drug.

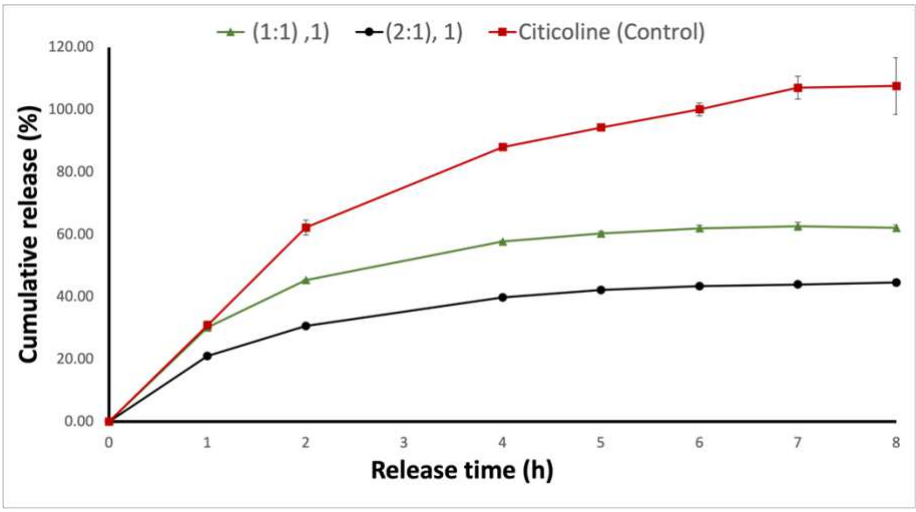

Figure 17: Release of citicoline over 8 h by membrane dialysis (DOPC: CH, Cit). Citicoline as control sample (red), (1:1), 1 (green) and (2:1, 1) (black).

2.4.5 NMR experiments

^{1}H NMR studies were carried out to confirm the presence of encapsulated drug molecules after purification. In Figure 18 the proton spectrum with assignment of citicoline 10^{-2} M in D_2O solution was reported. Table 6 reports the proton chemical shift values with multiplicity of signals. This experimental information is important to highlight the presence of citicoline in liposome and to identify the chemical position in the bilayer.

Table 6: ^{1}H NMR peak assignment of Citicoline molecule in D_2O.

Protons	a	b	c	d	e	f	g	h	i
Chemical shift (ppm)	7.89 (d,1H)	6.06 (d,1H)	5.93 (d,1H)	4.31 (d,1H)	4.25 (ddd,2H)	4.20 (S,1H)	4.13 (m,2H)	3.61 (m,2H)	3.16 (S,9H)

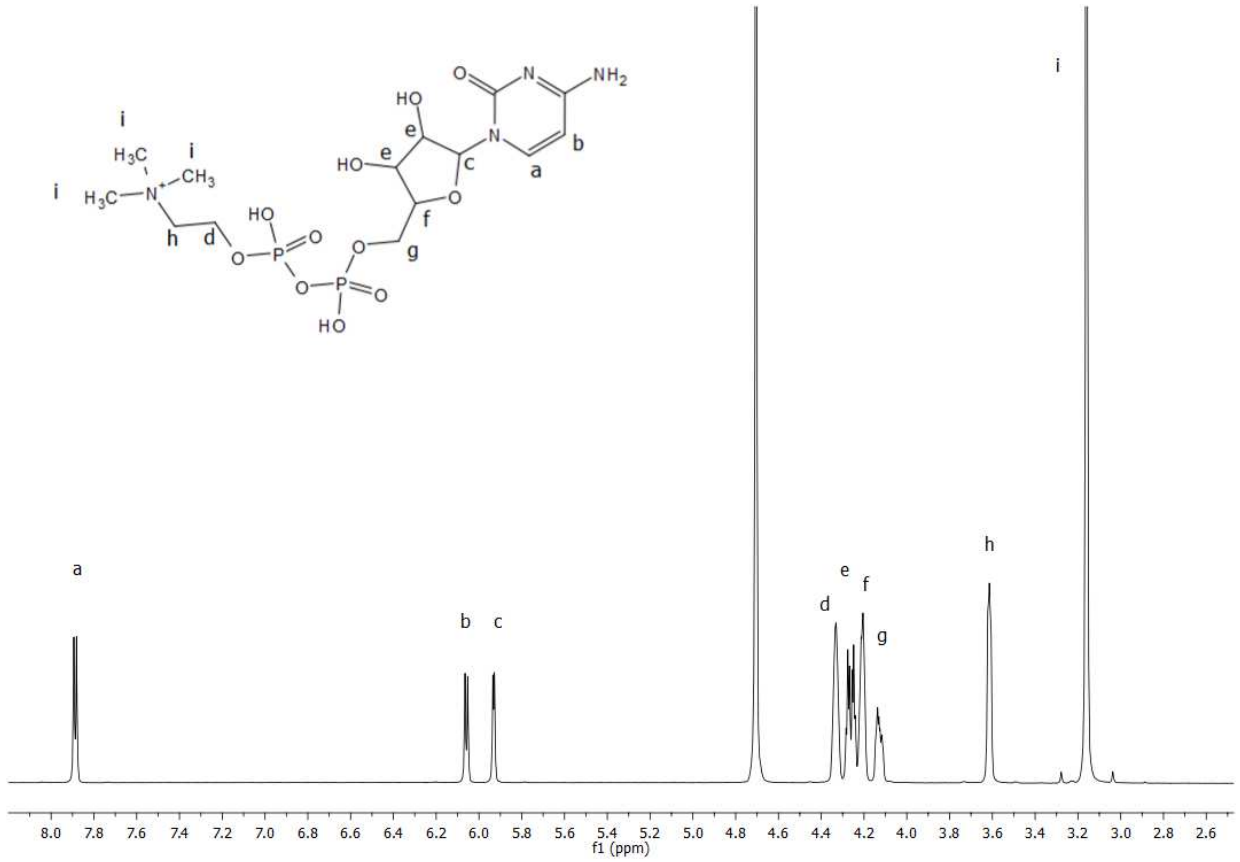

Figure 18: ^{1}H NMR spectrum of citicoline 10^{-2} M in D_2O with proton assignment.

Figure 19 shows the proton spectrum of the empty DOPC:CH (1:1) and DOPC:CH (2:1) liposomes, respectively. The DOPC proton assignment, obtained from literature was reported in Table 7. The first experimental evidence is the absence of any difference, in both chemical shift values and peak intensity, for two different liposome formulations. The presence of different concentrations of cholesterol modified the fluidity of bilayers without affecting the NMR spectra. A large NMR signal confirmed the presence of vesicles in the solution and the poor resolution of resonances was a typical characteristic of aggregates [62].

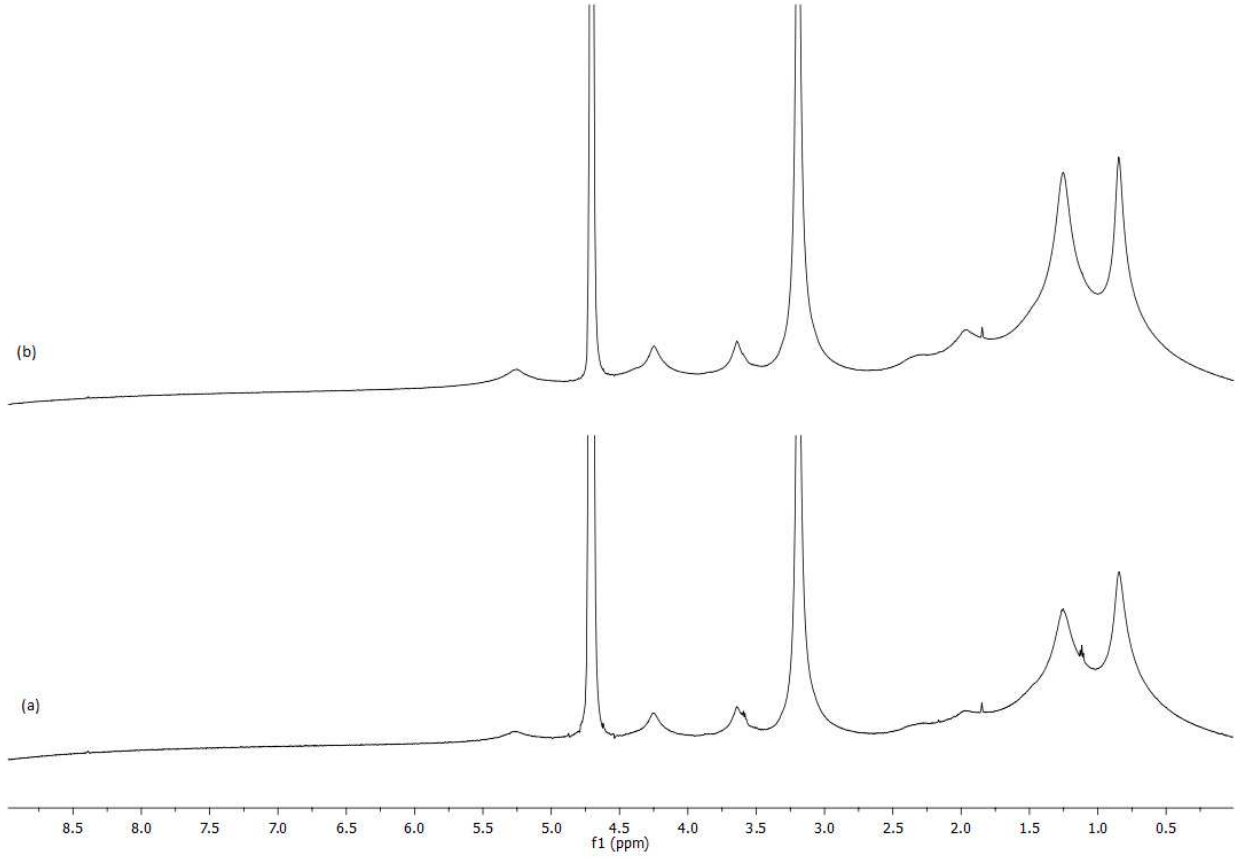

Figure 19: [1]H-NMR proton spectrum of empty liposomes: (a) DOPC:CH (1:1) and (b) DOPC:CH (2:1) in D2O recorded at 600 MHz and 298 K.

Table 7: 1H NMR peak assignment of DOPC molecule.

THE PEAK ASSIGNMENT: DOPC		
0.8 ppm	Methylenic protons of DOPC lipid tail	-CH2-
1.2 ppm	Methyl protons of DOPC lipid tail	CH3-
3.2 ppm	Methyl group of Lipid head	CH3-
3.6 ppm	Methylenic protons of DOPC lipid head (choline)	-CH2-
4.3 ppm	Methylenic protons in the glycerol part of the DOPC head	-CH2-, -CH

Figure 20 shows the comparison between loaded and plain liposomes DOPC:CH (2:1) and the spectrum of pure citicoline in solution. This approach allows to highlight the presence of the active compound in the liposomes. In the spectrum of liposomes loaded with the drug, low-field proton signals attributable to citicoline protons (H_a, H_b, H_c) can be seen after dialysis. In the molecule of citicoline, these peaks in the H-NMR spectrum correspond to the aromatic ring present in the cytidine portion. These aromatic peaks typically appear at low field, meaning they are observed at higher chemical shift values (upfield) in the H-NMR spectrum. The low-field shift of aromatic peaks in the H-NMR spectrum is primarily due to the electron-withdrawing nature of the aromatic ring. Aromatic compounds contain delocalized pi-electrons within the conjugated system of the ring. These pi-electrons create a local magnetic field that opposes the external magnetic field experienced by the nearby hydrogen atoms. As a result, the hydrogen atoms in the aromatic ring experience a slightly lower effective magnetic field, causing their NMR signals to shift upfield. The electron-withdrawing groups attached to the aromatic ring, such as nitrogen-containing functional groups in citicoline, further increase the deshielding effect and contribute to the low-field shift of the aromatic peaks. These electron-withdrawing groups pull electron density away from the ring, reducing the electron density available for shielding the nearby hydrogen atoms. In particular, the aromatic signals, H_a and H_b, indicate the insertion of citicoline into the hydrophilic head of the phospholipid bilayer and confirm the successful encapsulation of citicoline in the vesicles. Thus, the ^1H NMR data confirm the presence of citicoline in the liposomal system even after purification of the vesicles by dialysis procedures. These data are in agreement with the experimental values of the encapsulation efficiency of liposomes loaded with citicoline. The NMR study carried out on the DOPC:CH, Cit (1:1),1 liposome shows an identical behavior, suggesting

that different concentration of cholesterol not modify the insertion properties of drug in the liposomes.

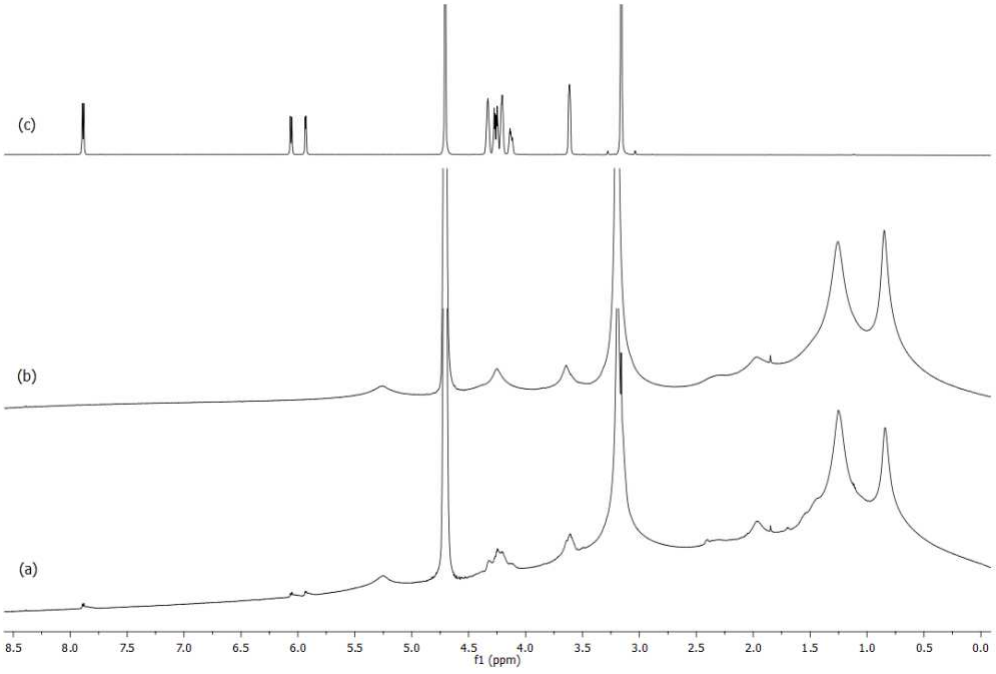

Figure 20: [1]H NMR spectra of liposomes: (a) DOPC: CH, Cit (2:1),1; (b) DOPC: CH (2:1) and (c) citicoline 10^{-2} M in D2O.

2.4.6 ATR-FTIR Studies

Pure citicoline, plain liposomes and citicoline-loaded liposomes were subjected to ATR-FTIR studies between 4000 cm^{-1} and 750 cm^{-1} to verify the association between citicoline water-soluble compounds and phospholipids analyzing the frequency of different vibrational modes. The loaded samples were subjected to purification prior to the experiment to remove the interference of water and free active molecule. Figure 21(a) and Figure 22(a) show the spectra of a DOPC: CH before and after loading citicoline with two different molar ratios of DOPC and Cholesterol, 1:1 and 2:1, respectively. Magnification of the spectra of 1700-1000 cm^{-1} region is shown in Figure 21(b) and Figure 22(b) presenting the most relevant bands.

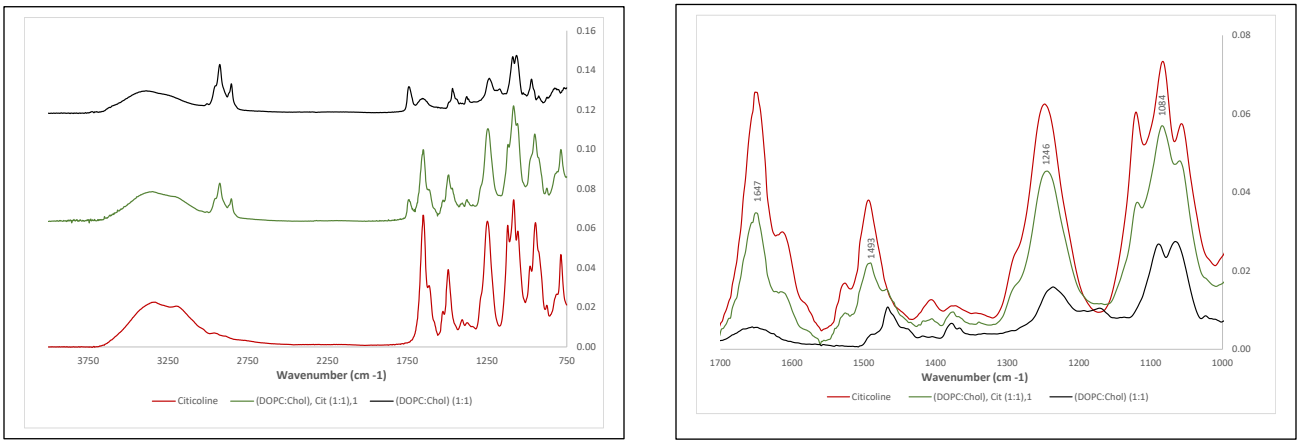

Figure 21: FTIR-ATR spectrum for a) stacked(left) b) overlapped (right) in region 1700-1000 cm-1 of DOPC: CH(1:1) (black); (DOPC: CH), Cit (1:1),1 (green); and Citicoline (red).

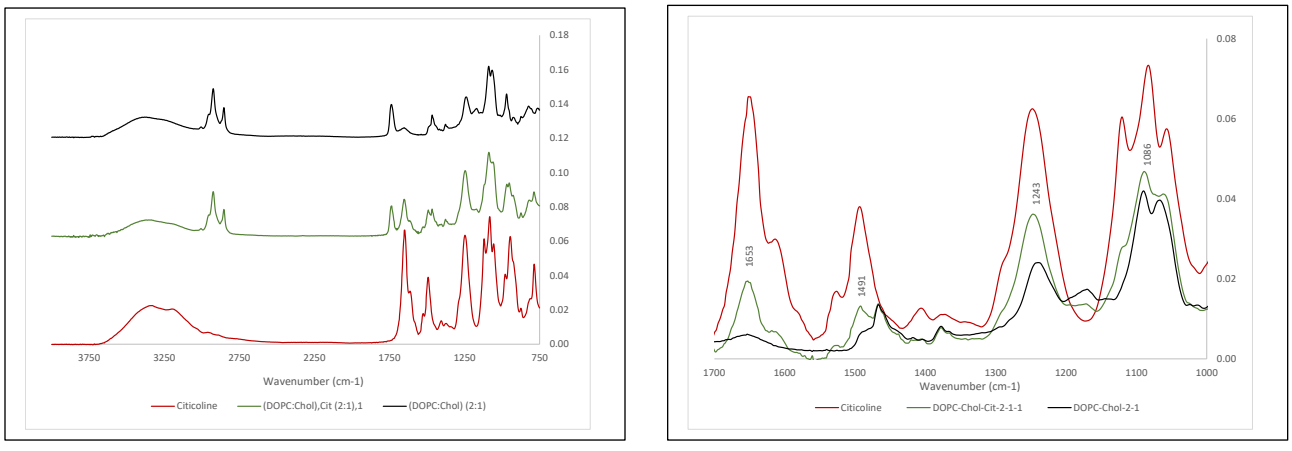

Figure 22: FTIR-ATR spectrum for a) stacked (left) b) overlapped (right) in region 1700-1000 cm-1 of DOPC: CH(2:1) (black); (DOPC: CH), Cit (2:1),1 (green); and Citicoline (red).

The main absorption bands and their assignment are listed in Table 8 [63,64]. The presence of citicoline in the purified liposomal formulation is confirmed by characteristic bands attributed to the active compound in the spectra of drug loaded liposomes, as the NH_2 wagging motion at 787 cm^{-1}, the appearance of a shoulder at 1117 cm^{-1}, as a component of the corresponding adsorption band of citicoline due to the stretching of C-O ether bond.

Table 8: Main bands and assignment observed in FTIR spectra of plain liposomes and citicoline.

Wavenumber (cm^{-1})	**Vibration**	**Sample**
3006	Stretch. =C-H	Plain liposomes
2920-2850	CH_2 stretch.	
1750	C=O ester stretch.	
1652	C=C stretch.	
1243	PO_2^- antisymm. stretch., C-O-C stretch.	
1091	PO_2^- symm. stretch.	
970	$C\text{-}N^+\text{-}C$ antisymm stretch.	
3250	-OH stretch.	Citicoline
1653	Cytosine C=O stretch	
1652	C=C stretch.	
1491	Cytosine C=N	
1243	PO_2^- antisymm. stretch.	
1091	PO_2^- symm. stretch.	
1117	C-O ether stretch.	
970	$C\text{-}N^+\text{-}C$ antisymm stretching	
926	$C\text{-}N^+\text{-}C$ symm stretching	
787	NH_2 wagging	

2.4.7 ToF-SIMS Measurements

TOF-SIMS analysis was performed to support NMR and IR data. Samples were cast on a silica surface and were dried under nitrogen flow. Figure 23 reports characteristic fragments of citicoline, which are identified as m/z 112, corresponding to the cytosine moiety of the molecule (cytosine+$2H^+$) m/z 227, ($C_9H_{12}N_3O_4^+$) m/z 353 ($C_{13}H_{11}N_2O_6P_2^+$) m/z 381 ($C_9H_{10}N_4O_{11}P^+$). Figure 24 reports the spectral region between 100 and 400 m/z, where the choline moiety (m/z 104) and the cytosine ion from citicoline are labeled. The presence of citicoline in the liposomal preparation is identified by the presence of the ion at m/z 112, as the other fragments are reproducible both to DOPC or cholesterol (Figure 25).

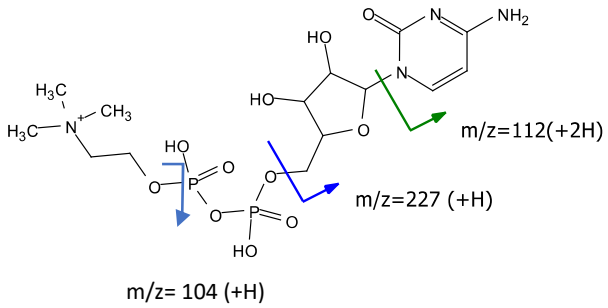

Figure 23: Structure and characteristic fragments of Citicoline.

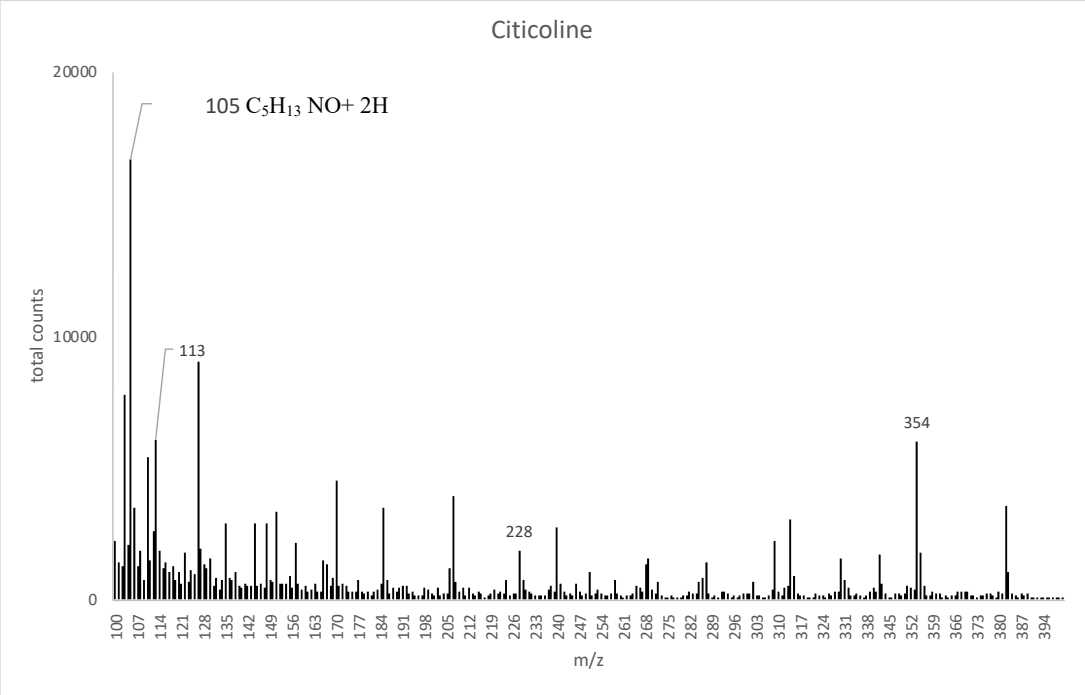

Figure 24: ToF SIMS positive ion spectra of citicoline (m/z range 100-400).

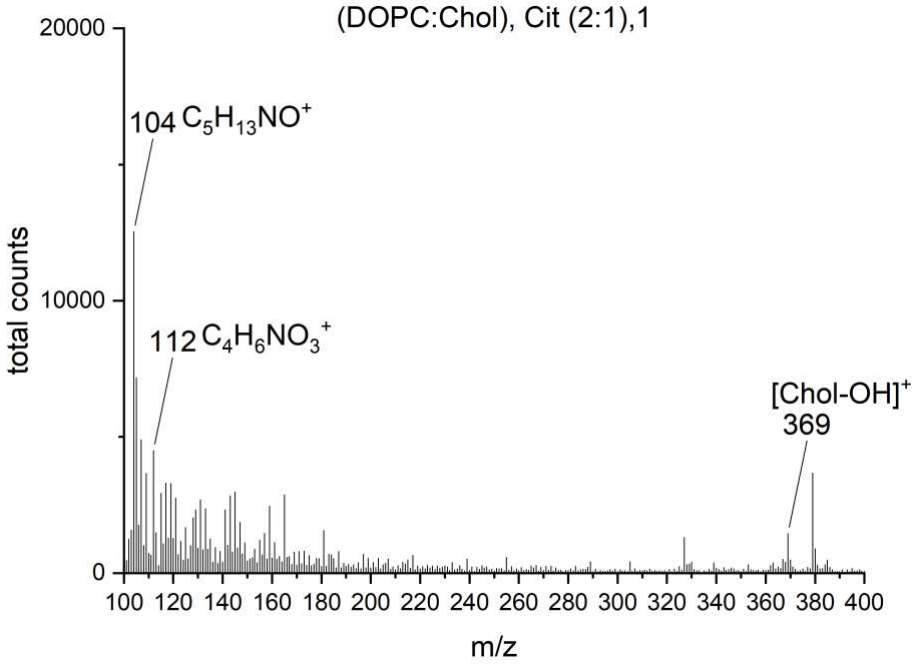

Figure 25: ToF SIMS positive ion spectra of (DOPC: CH), Cit (2:1),1, (m/z range 100-400).

2.4.8 Physical stability of liposomes loaded with citicoline versus time

The liposome is a system of thermodynamic instability, its physical and chemical properties may change during storage. The vesicles may gather and fuse, leading to the drug's leakage and the particle size increase over the storage period. The present study evaluated the mean size and PDI value of plain and loaded liposomes, stored at 277 K in PBS solution for 3 months, and their stability versus time. Figure 26 reports the hydrodynamic size for all plain and loaded liposomes recorded versus time (0, 30 and 90 days). None of the liposomal formulations showed significant changes in hydrodynamic size within 3 months, suggesting that the liposomes were sufficiently stable and that the aggregation/flocculation processes not modified the physical-chemistry properties. Similar evidence can be obtained by analyzing the PDI parameters versus time. As reported in Figure 27 the PDI value remains stable around 0.20 for empty liposomes and increases up to 0.35 for the vesicles containing citicoline. This suggests that empty liposomes are stable over time and relatively monodisperse, while citicoline liposomes showed a PDI of 0.30-0.35 which can be acceptable and indicates a homogenous population of phospholipid vesicles. Moreover, the different cholesterol content in the two liposomal formulations does not affect the stability of the vesicles in the PBS solution.

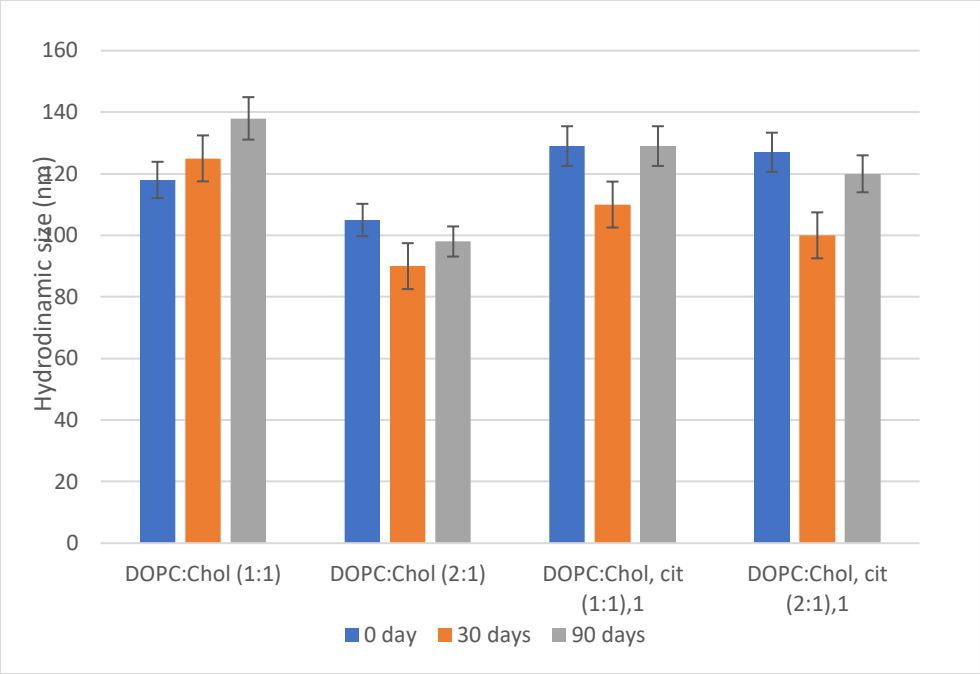

Figure 26: The hydrodynamic size of plain and loaded liposomes over three months (average error 5%).

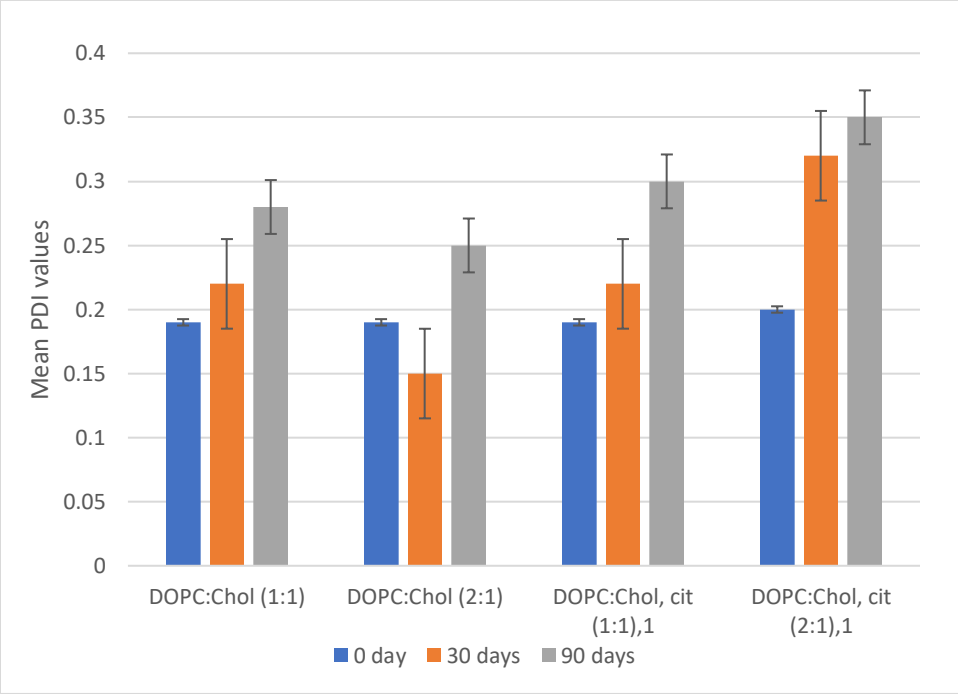

Figure 27: Mean PDI values over three months (average error 5%).

2.3.8 Biological characterization: In vitro viability test

For the neutral red uptake (NRU) viability test, NIH_3T_3 fibroblasts (controls) and cells were seeded in 24-well plates. Cells were maintained at 37 °C, 5% CO_2 in a humidified atmosphere for 24 hours before the performance of the NRU assay. The NRU tests were applied to determine the viability of cells after being cultivated at different concentrations in the presence of liposomal systems, which revealed no cytotoxic effects on NIH_3T_3 fibroblasts. As shown in Table 9, the level of cell viability on the whole-time axis (> 97%) remained above 70%, defined by the European standard (ISO DIN EN ISO 10993–5) as the lowest threshold for cytocompatibility. Therefore, the results on NIH_3T_3 fibroblasts confirmed the non-cytotoxic properties of liposomal systems loaded with citicoline.

Table 9: Percentage of viable NIH3T3 after 24 hours of contact with increasing concentrations of test samples. The Neutral Red Uptake test determined cell viability. Results are reported as a percentage of viable cells ± SD. No value is different compared to the negative control (complete medium), p<0,01.

Samples	0.1 (% v/v)	1 (% v/v)	5 (% v/v)
DOPC:CH, Cit (1:1), 1	101 ± 5	103 ± 6	97 ± 2
DOPC:CH, Cit (2:1), 1	98 ± 3	102 ± 4	98 ± 5

2.4 Conclusions and recommendations

Citicoline (CDP-choline; cytidine 5′-phosphocholine) was capsulated into two different liposomal formulations DOPC: CH (2:1) and (1:1) liposomal carrier to improve its therapeutic effects. The citicoline-encapsulation efficiency, drug leakage and size analysis of various liposome systems were studied. Small polydispersity of the prepared liposomes indicated a promising dispersion homogeneity (<0.2), suggesting that all liposomes are relatively monodisperse. The EE % for the two liposome formulations DOPC:CH, Cit (1:1), 1 and DOPC:CH, Cit (2:1), were above 40%. It can be concluded that the zwitterionic liposomes are good systems for the encapsulation of a hydrophilic drug such as citicoline. The experimental results showed that the formulation DOPC:CH, Cit (1:1),1 reaches a plateau more rapidly than the formulation DOPC:CH, Cit (2:1),1. Cholesterol concentration affects the release process of citicoline in physiological fluid. In other words, the higher cholesterol concentrations slowed down the release of the drug. The study of the hydrodynamic size of liposomes revealed a sufficient stability. This suggests that empty liposomes are stable over time and relatively monodisperse, while citicoline liposomes showed a PDI of 0.30-0.35 which can be acceptable and indicates a homogenous population of phospholipid vesicles. Moreover, the different cholesterol content in the two liposomal formulations did not affect the stability of the vesicles in the PBS solution. At the end, the results on NIH_3T_3 fibroblasts confirmed the non-cytotoxic properties of liposomal systems loaded with citicoline. The future perspective of ocular drug delivery using citicoline in liposomal encapsulations holds significant promise for addressing various ocular conditions. Here are some potential future directions and challenges:

a. Targeted Drug Delivery: Developing targeted delivery systems that specifically deliver citicoline to the desired ocular tissues or cells will be a key focus. This may involve surface

modification of liposomes with ligands or receptors that facilitate active targeting, enabling precise drug delivery and maximizing therapeutic effects.

b. Combination Therapy: Exploring the potential of combining citicoline with other drugs or therapeutic agents in liposomal formulations could provide synergistic effects and enhanced treatment outcomes. Combinations may target multiple pathways or address different aspects of ocular diseases, leading to improved therapeutic efficacy.

c. Overcoming Ocular Barriers: The ocular barriers, such as the cornea, conjunctiva, and blood-retinal barrier, pose challenges for drug delivery. Strategies to enhance the penetration and permeability of liposomal formulations containing citicoline will be explored, including the use of penetration enhancers, mucoadhesive systems, or physical techniques like iontophoresis.

Chapter 3: The effect of FT-PVA particles on the mechanical properties of methacrylate chondroitin sulfate hydrogel

3.1 Introduction

Three-dimensional (3D) polymer networks known as hydrogels are distinguished by their high-water content and, hence, considerable brittle. As a result of their water content, they naturally resemble various biological tissues. Hydrogels can be comparable to soft tissues in terms of

their mechanical characteristics. Together with other desirable qualities like biocompatibility, functionality, and reversibility, their viscoelastic nature minimizes harmful mechanical irritation of the surrounding host tissue after implantation, making them a crucial and incredibly fascinating component of the biomaterial group [65,66]. High water-based liquid absorption is made possible by hydrophilic groups in the hydrogel polymer network. The hydrogel swells and expands as its water content rises. The hydrogel structure determines the number of free water molecules present; the more compact the structure, the fewer free water molecules are present. While intermediate water is produced by weak interactions between the functional groups of polymer chains and water molecules, bound water is produced by strong hydrogen bonds between the polymer and the water molecules. Crosslinking, which involves connecting molecules, often enhances mechanical qualities and increases hydrogel stability. Furthermore, it reduces polymer degradability and the number of accessible functional groups, limiting modification options [67]. In situ cross-linkable hydrogels have found widespread application as therapeutic implants and platforms for tissue engineering and regenerative medicine. In situ forming hydrogels are made by cross-linking a wide range of natural and synthetic polymer biomaterials. With the help of various physical and chemical stimuli, these polymers undergo a phase shift from a solution to a gel state. They can encapsulate therapeutic materials (for example, drugs, proteins, cells, and genes) following hydrogel creation and be delivered to the target areas utilizing injectable devices [68]. Despite having weak mechanical qualities, natural polymers like polysaccharides have the benefits of low toxicity and biodegradability. Since synthetic polymers tend to be hydrophobic and mechanically more robust than natural polymers, hydrogels made from synthetic polymers have better endurance and delayed breakdown. Synthetic polymers also have an inert cellular environment, which prevents active cell binding and lowers cell survival. For a given hydrogel application, the opposing qualities of synthetic and natural polymers need to be balanced through optimal design [69,70].

Synthetic PVA is a strong polymer that has been used in hydrogels since 1970 for different applications. PVA hydrogels were formed in this study by freeze-thaw cycling, a physical crosslinking method. Physical crosslinking takes place through noncovalent connections, including electrostatic interactions, hydrophobic interactions, and van der Waals forces. The freeze-thaw method forms polymer crystals in repeated freezing and thawing cycles, which act as crosslinks creating elastic properties and a high swelling degree in water. The fraction of crystalline regions within the hydrogel also increases as the number of cycles increases, creating a stronger structure. The hydrogel created by this approach is also a useful delivery medium for cells and bioactive compounds [71]. In this study, chondroitin sulfate was methacrylated to be chemically crosslinked via UV light. The incorporation of FT-PVA particles to methacrylate chondroitin sulfate was hypothesized to improve mechanical modulus by adding physical crosslinking to the hydrogel. Different prepolymer concentrations and crosslinking conditions were applied to optimize this objective.

3.2 Experimental

3.2.1 Materials

Deuterated dimethylsulfoxide (DMSO-d_6) was purchased from Cambridge Isotopes (Tewksbury, USA). Bovine chondroitin sulfate (M_n 50 kg/mol, >90% purity) was purchased from LKT. Methacrylic anhydride, D_2O, sodium hydroxide, 2-hydroxy-4′-(2-hydroxyethoxy)-2-methylpropiophenone (Irgacure 2959), and poly(vinyl alcohol) (PVA, M_w 85000-124000 g/mol, 99% hydrolyzed) were all obtained from Sigma- Aldrich, Ltd., Canada. The water used was of type 1 purity, obtained from a Millipore Milli-Q plus ultra-pure water system.

Chondroitin sulfate purification

Chondroitin sulfate (CS) was dissolved in Milli-Q water at a concentration of 10 mg/ml and filtered by a 0.45 μm filter to remove insoluble impurities. The filtrate solution was dialyzed against water using a 3.5 kDa molecular weight cut-off membrane for 48h, with water changes every 12 h. The chondroitin sulfate solution was frozen in liquid nitrogen and lyophilized for 48-72h to obtain purified CS.

3.2.2 Methacrylation of chondroitin sulfate

Briefly, CS (1 g, 2.16 mmol) was dissolved in Milli-Q water (50 mL) to reach 2% w/v% solution at RT (Figure 28). Methacrylic anhydride with two different excess molar ratios (5 and 12) was added dropwise (over 1 h) while continuously adjusting the pH between 8–9 (1 M NaOH). Next, the reaction mixture was concentrated for 24-48 h under air flow to increase the synthesis yield during the precipitation process. Then it was followed by precipitation in cold acetone and keeping the solution in the freezer at -20 ºC overnight to increase the synthesis yield. After 2 min centrifugation, a white precipitant was recovered, redissolved in Milli-Q water with 10% concentration (initial weight of CS w/v%), and dialyzed against water for 2 days (membrane cut-off 3.5 kDa). The final product, referred to as methacrylate CS (CSMA), was obtained after freeze-drying for 2 days. Finally, a white, cotton-like material (yield ~51%, defined as the ratio between the mass of the recovered CSMA and the starting CS) was collected.

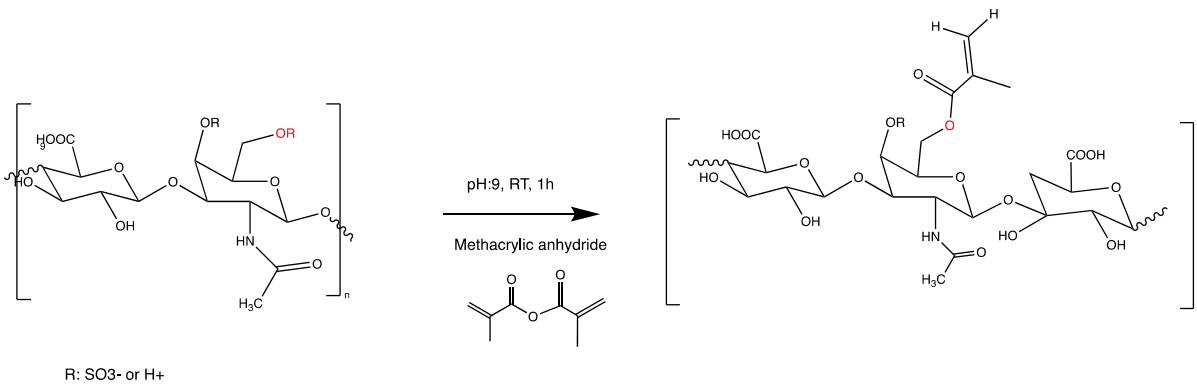

Figure 28: Overview of methacrylation mechanism of CS.

3.2.3 Micronization of FT-PVA

Probe sonication is commonly used for micronization in various fields, including pharmaceuticals, nanotechnology, biotechnology, and materials science. One common advantages of this method is the ability to achieve uniform particle size reduction. This technique is used to reduce the particle size of materials through the application of high-frequency sound waves that propagate through a liquid medium containing the material to be micronized. 50 ml stock PVA 5% (w/v%) was prepared at 80°C for 3 h in Milli-Q water on the magnetic stirrer. 500 µl of PVA solution was cast in triplicate in a multiwell plate and shaken on a shaker for 1 h to remove the bubbles. The samples were then exposed to one to eight cycles of freezing for 20h at-20°C and thawing for 4h at RT. The FT-PVA discs were frozen in liquid nitrogen and lyophilized for 48 h. FT-PVA samples with at least three FT cycles formed a stable and strong gel. FT-PVA with four FT cycles was lyophilized and reduced in size as described in previous studies with slight modifications [72][73]. Briefly, the discs initially were ground with a pestle and mortar. Then they were dispersed in acetonitrile at a maximum concentration of 4% w/v and vortexed at 800 rpm for 2 min. Samples were kept in a dry ice bath (isopropyl + dry ice, -80°C) for 20 s to prevent warming and vortexed for 2 min. Following 30 s freezing in dry ice the suspension was gently sonicated using a 9 W Fischer Scientific 100 probe sonicator for 2 min while being kept in an ice bath. This cycle was repeated five times (Figure 29). The size of FT-PVA particles was measured using a Zeiss Axio M1 microscope in transmission mode.

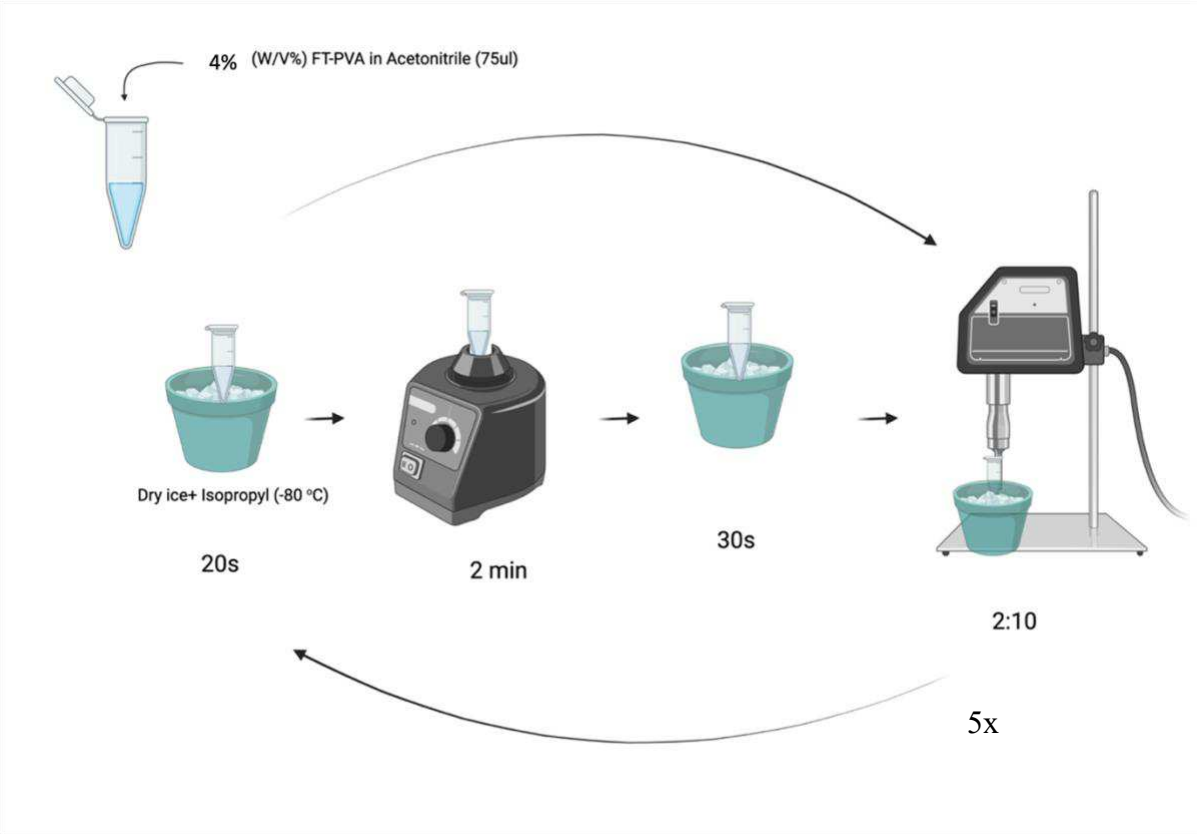

Figure 29: Schematic of equipment set up for the formation of micro-sized FT-PVA. Created with BioRender.com.

3.2.4 Hydrogel formation

To prepare hydrogels with different Young's moduli, various conditions such as prepolymer concentration, degree of methacrylation and FT-PVA concentration were examined prior to photo-crosslinking. The effect of these parameters on sol content, water content, and mechanical stiffness of the hydrogel was studied. Briefly, the CSMA hydrogel disks were prepared by dissolving the CSMA in Milli-Q water at varying concentrations (5-20 wt%). The resulting polymer solutions with and without FT-PVA particles were supplemented with Irgacure 2959 photoinitiator (0.1- 0.3% w/v final concentration,). 50 µl of the mixture was injected into a 1 ml syringe mold. The dimensions of the gels were about 2*3 mm (diameter *height). The cross-linking was achieved by UV-irradiating the samples for different times (3-6 min) on each side of the mold (UV lamp LC8, Hamamatsu) with an intensity

range of 25-35 mW/cm^2, wavelength 365 nm to find the most suitable crosslinking condition (Figure 30).

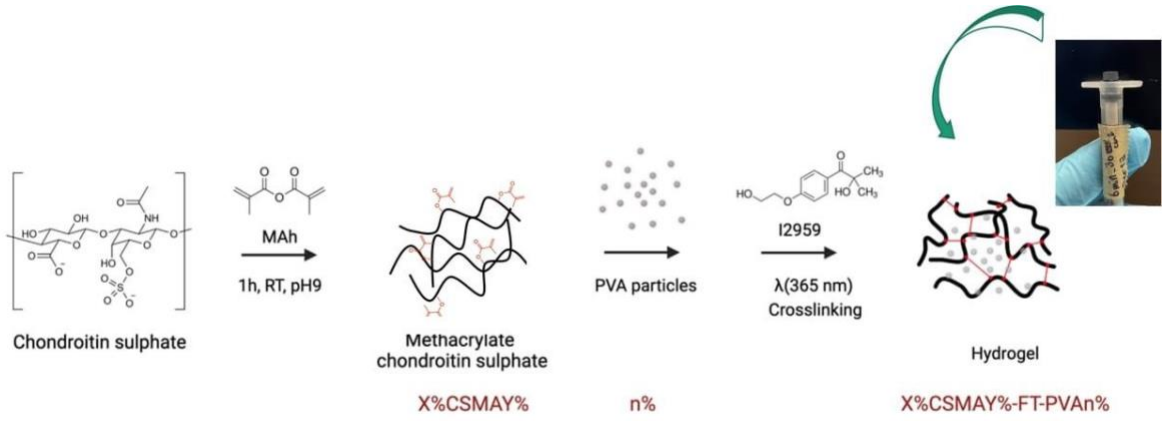

Figure 30: Schematic of CSMA hydrogel formation containing FT-PVA particles, (X: DM, Y: concentration of prepolymer w/v%, and n: concentration of FT-PVA w/v%)

3.2.5 Polymer characterization

The most used analytical method applied to determine the degree of methacrylation (DM) of CSMA is ^{1}H-NMR analysis. Polymer compositions were confirmed from ^{1}H-NMR spectra obtained in DMSO-d_6 and D_2O on a Bruker Avance 400 MHz NMR spectrometer. Detailed peak assignments and ^{1}H-NMR spectra analyses can be found in FigureA2- 1 to FigureA2- 6. ^{1}H-NMR spectra of the prepolymers were collected from 0.7 mL samples dissolved at 30 mg/mL. Usually, the intensity of the signals of the vinyl groups (signals can typically be found around ~5.8 and 6.2 ppm) of the methacrylate groups is quantified and compared with a known peak in the spectrum. In the vinyl group (-CH=CH2), the presence of the double bond creates a region of increased electron density above and below the plane of the molecule. This increased electron density affects the local magnetic field experienced by the nearby protons. The pi electrons in the double bond create a shielding effect, reducing the effective magnetic field experienced by the protons and causing them to shift downfield (to lower chemical shift

values) in the NMR spectrum. Sometimes, the DM is also quantified by quantifying the methacrylate methyl peak (at ~1.9 ppm). This quantification typically leads to an overestimation of the DM, due to the overlap of this peak with other CS-related proton peaks [74]. The ratio of the average integrated region of the double bond protons (A (H) and A (H')) to the integrated region of the anomeric proton of CS was used to calculate DM per repeating unit on CSMA using equation (3).

(3)

$$DS\ (\%) = \frac{[A\ (H) + A\ (H')]/2}{Known\ peak\ integration\ (Normalized\ to\ 1)} * 100$$

3.2.6 Hydrogel characterization: Sol Content and Water Content

Cross-linking efficiency was assessed through the measurement of the sol content for all hydrogels (n = 3). Immediately after photo-crosslinking, the gels were first frozen in liquid nitrogen. The frozen gels were lyophilized, and their dry initial mass was recorded. The gels were soaked in water at RT for 24 h, with the water replaced thrice. The gels were again frozen in liquid nitrogen, lyophilized, and their final dry mass was recorded. The sol content was calculated using equation 4.

(4)

$$Sol\ content(\%) = (\frac{Mass\ dry, initial - Mass\ dry, final}{Mass\ dry, initial}) \times 100$$

Water content was determined by soaking of the hydrogels in pH 7.4 phosphate-buffered saline (PBS) for 24h at RT. The surface moisture was removed by blotting using Kim wipes to remove surface water and weighed (wet mass). They were frozen and the water was removed by

lyophilization and weighted (dry mass), and the water content was determined using equation 5.

(5)

$$Water\ content(\%) = (\frac{Mass\ wet - Mass\ dry}{Mass\ wet}) \times 100$$

3.2.7 Measurement of mechanical properties

The hydrogels were formed into a 1 ml syringe, confined with two stoppers from two ends to form a flat surface. The diameter of the hydrogels was measured using calipers immediately before testing. The mechanical properties were measured using a CellScale UniVert system (Waterloo, Canada) equipped with a 10 N load cell, and a fixed bottom platen and the hydrogel samples were kept at 37°C in a PBS of pH 7.4 bath throughout testing. The viscoelastic mechanical properties of the hydrogels were assessed using compression stress relaxation tests. Unconfined hydrogel samples (n=3) were fully submerged in PBS and a 1%/s strain rate was applied up to 90%. Peak stress (kPa) and strain at failure (%) were reported at the point of hydrogel failure. The instantaneous modulus was determined from the same curves by measuring their slope from 0 to 5%. Stress-relaxation experiments were conducted with rate of 5%/s up to 25-30% strain to determine the equilibrium modulus of each sample. The resulting force decay was recorded until equilibrium was reached, and the linear regression at equilibrium was recorded to obtain the equilibrium modulus for each hydrogel. The hydrogel response to repeated compressions was tested by applying continuous compression-relaxation cycles under 20% strain at a rate of 1%/s to the same hydrogels for 20 cycles without any waiting time between each cycle. The slope of the linear regions between 2-8% strain in each

cycle was extracted to provide a measure of the hydrogel's stability under 20-cycle compression.

3.2.8 Statistics

A one-way ANOVA with a Tukey post-hoc analysis for multiple comparisons was run to determine significant differences between hydrogels with and without incorporated FT-PVA particles using GraphPad Prism 9.5.1. A comparison with a p-value greater than 0.05 was accepted as not significantly different.

3.3 Results and Discussion

3.3.1 Polymer characterization

The molar feed ratio of methacrylic anhydride (MAh) to CS repeating units and the final degree of methacrylation for all hydrogels were calculated from the ^{1}H-NMR spectra (Figure 31 and Figure 32). Two different degrees of methacrylation were obtained (5%, and 16%) for 5 and 12 times molar excess MAh, respectively.

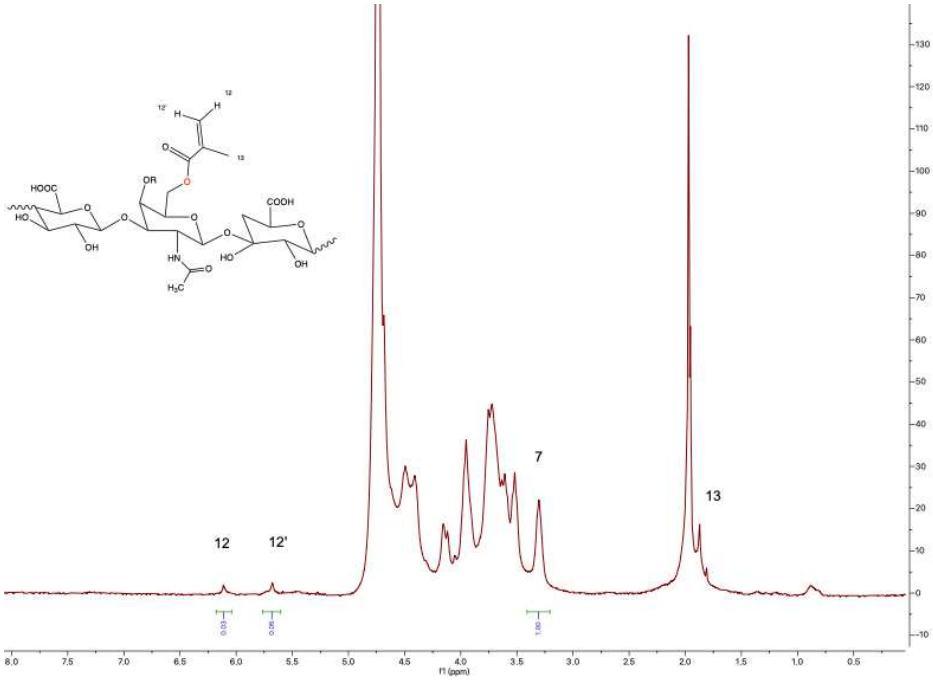

Figure 31: Representative 1H-NMR spectrum (D_2O, 400 MHz) of the methacrylate chondroitin sulfate CS: MAh 1:5 excess molar ratio

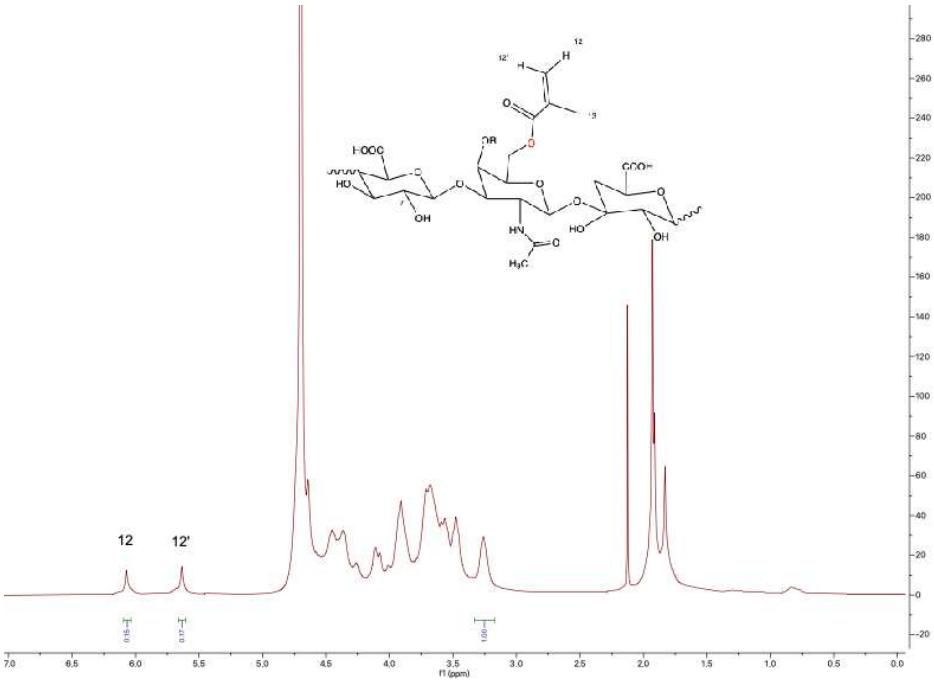

Figure 32: Representative 1H-NMR spectrum (D2O, 400 MHz) of the methacrylate chondroitin sulfate CS: MAh 1:12 excess molar ratio

3.3.2 FT-PVA particle size measurement

The size FT-PVA particles with 4 cycles after micronization processing was characterized using Zeiss Axio M1 microscope in transmission mode. The FT-PVA particles were collected on glass slides and following solvent evaporation, the average diameter of about 20 single fraction particles was measured using ImageJ software 1.52v which approximately was 15 µm± 5 (Figure 33).

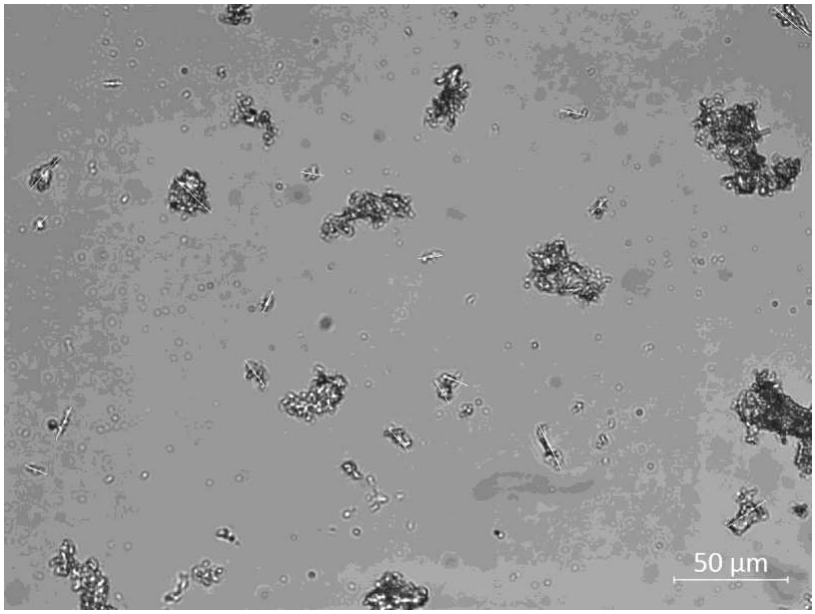

Figure 33: Average particle size of 4FT-PVA microparticles under the microscope from the longest axis.

3.3.3 Hydrogel formation

Different concentrations of the prepolymer with two different degrees of methacrylation were crosslinked and tested. A higher prepolymer concentration of CSMA (20 w/v%) with 16% DM was selected to be crosslinked (Table 10). The samples with a lower degree of methacrylation

were too soft and unstable and were not easy to work with (Table 11). An increase in prepolymer concentration in the solution causes an increase in polymer chain entanglement, allowing the hydrogel to retain its form and not break apart. The hydrogel prepared using a 10% prepolymer concentration did not form a cohesive hydrogel and was brittle. In contrast, the hydrogel prepared with a 20% prepolymer concentration formed a cohesive hydrogel that could be readily handled. Furthermore, varying photocrosslinking conditions were examined (Table 12). The cross-linking done with lower intensities of light (25 mW/cm^2) and a shorter irradiation time formed weak gel-like materials that were non-cohesive and difficult to handle. Afterward, the concentration of the photoinitiator was increased from 0.1% to 0.3%, but this caused a brittle hydrogel to form. Increasing the amount of initiator in a free radical polymerization resulted in more chains getting initiated. This causes a shorter average kinetic chain to be formed, consequently, an increase in the crosslinking density of the hydrogels and as a result an increase of modulus. The intensity range of 30-35, and for 5-6 min irradiation with 0.1% photoinitiator made the hydrogels with similar mechanical properties. The hydrogels were cross-linked at the optimum condition which was 30 (mw/cm^2) for 5 min on each side. The water and sol content of hydrogels with and without FT-PVA particles were measured and are listed in Table 13. Articular cartilage itself has a high-water content ranging from 60% to 90% by weight. Therefore, hydrogels designed for articular cartilage treatment often aim to achieve water contents that closely resemble the native cartilage environment. This range allows for sufficient hydration and provides a favourable environment for cell viability, nutrient transport, and tissue regeneration. The control hydrogel (16%CSMA20%) had the most water content which was 94%. This value was about 90% for all other formulations. Cross-linking efficiency was assessed through the measurement of the sol content. Sol content refers to the amount of unreacted or uncross-linked material that remains in the hydrogel after the cross-linking process. It represents the fraction of polymer chains that did not participate

in the formation of the hydrogel network. The sol content is typically expressed as a percentage of the total polymer mass. A lower sol content indicates a higher degree of cross-linking and a more complete conversion of the polymer into the hydrogel network. This is desirable for hydrogels used in articular cartilage applications, as it ensures a higher mechanical integrity and reduces the risk of unwanted leaching or release of unreacted components into the surrounding tissue. The sol content can be controlled by adjusting the cross-linking conditions, including the cross-linking agent concentration, reaction time, and temperature. Optimization of these parameters is crucial to achieve a low sol content while maintaining the desired properties of the hydrogel. Sol content values indicate that the crosslinking efficiency was relatively high as they are less than 10%. Although the hydrogels with incorporated FT-PVA particles resulted in a lower crosslinking efficiency that might be due to blocking of the UV light in photo crosslinking process, especially in higher concentrations of FT-PVA particles.

Table 10: Used excess molar ratio vs. DM (%) of CSMA.

Excess molar ratio MAh:CS	Methacrylation degree (%)
5:1	5
12:1	16

Table 11: Preparation of the best X%CSMAY% formulation hydrogel. X% is the degree of Methacrylation, and Y% is the prepolymer concentration (w/v%).

X%CSMAY%	X%	Y%	Mechanical properties
	Methacrylate Degree	**Prepolymer concentration (w/v%)**	
5%CSMA10%	5%	10%	Too soft and weak
5%CSMA20%	5%	20%	Too soft and weak
16%CSMA10%	16%	10%	Brittle
16%CSMA20%	16%	20%	Well-formed gel

Table 12: Crosslinking conditions and corresponding crosslinking time.

Intensity (mW/cm^2)	Time (min)	I2959 concentration (w/v%)	Mechanical properties
25	3	0.1%	Did not crosslink
30-35	5-6	0.3%	Brittle
30-35	5-6	0.1%	Well-formed gel

Table 13: Water and sol content of the hydrogels were soaked in pH 7.4 PBS for 24h at RT. 16%CSMA20%-4FT-PVAn%, 16% is the MD, 20% is the prepolymer concentration (w/v), n% is the concentration (w/v) of FT-PVA in hydrogels.

16%CSMA20%-4FT-PVAn%	Water content	Sol Content
16%CSMA20%	94%± 3	3%± 1
4FT-PVA 5%	89± 1	------
16%CSMA20%-PVA0.3%	91%± 0	6% ± 1
16%CSMA20%-PVA0.5%	90%± 2	7%± 1
16%CSMA20%-PVA1%	89± 1	10%± 1

3.3.3 Mechanical Properties

The instantaneous, linear, and equilibrium moduli of CSMA (control) and 16%CSMA20%-FT-PVAn% (n= 0.3%, 0.5% and 0.10%) hydrogels (n=3 or 4) were measured in unconfined compression mode (Table 14). FT-PVA hydrogels showed a low instantaneous modulus and a viscoelastic behaviour which could resist higher strain% without damage (Figure 34). An example of the stress-strain curves for chondroitin sulfate hydrogels can be seen in FigureA2-7. The hydrogel made with 1% FT-PVA failed at a lower strain value compared to other formulations (Figure 35). This result is due to the brittleness of this hydrogel formulation. Failure occurred at around 35% strain in the CSMA control hydrogel and 45% strain when 0.5% FT-PVA was added to the hydrogel. The stress and strain at failure were extracted from stress-strain curves shown in Figure 35. However, focusing on stress and strain at failure is not recommended because comparing these two values requires a defect-free sample. The manufactured hydrogels with a little surface crack fail easily because the concentration of energy at the crack point causes crack propagation. The instantaneous modulus of the hydrogels

was compared with each other (Figure 36). The hydrogel with 1% incorporated FT-PVA particles was highly improved compared to the control sample and reached about 730 ± 178 kPa. This result indicates that the addition of FT-PVA particles can affect Young's (instantaneous) modulus. This might be due to physical cross-links between FT-PVA and the CSMA in the form of hydrogen bonds, which increase the molecular interaction in hydrogel and the strength of the gel structure. This result is also in agreement with the brittle feature of the hydrogels with 1% FT-PVA. The equilibrium moduli obtained from stress relaxation tests were approximately in the range of instantaneous moduli and increased with incorporation of FT-PVA to a maximum concentration of 0.5% (Figure 37). Since 16%CSMA20%-PVA 1% hydrogel was more brittle than others it was not able to be tested for this experiment. An example of the extraction of equilibrium modulus from stress relaxation curves can be seen in FigureA2- 8. The loading-unloading was tested by applying subsequent compression-relaxation cycles under 20% strain to the same hydrogels for 20 cycles without any waiting time between each cycle. To facilitate the display of hysteresis loop morphological characteristics, FigureA2- 9 , as an example, shows only the 1^{st}, 5^{th}, 10^{th}, 15^{th}, and 20^{th} cycles. Comparing these two graphs shows that the control hydrogels (16%CSMA20%) hysteresis loop is continuously experiencing a shift to a higher stress level in each cycle. This may indicate that the sample had not fully recovered after each cycle and still felt some stress which increased in the next cycle. But in the sample with PVA particles, relaxation occurred more quickly and there was no effect on stress value of the next cycles. In addition, the slope of each loop in a linear region of 2-8% was extracted and plotted in Figure 38. According to the results, the hydrogels were not damaged, and values did not change significantly. This result demonstrates the stability of hydrogels after the 20 cyclic compressions.

Table 14: The mechanical properties of hydrogel in PBS (Load cell 10N) at 37 ˚C. NA indicates that the experiments did not perform due to the brittleness feature of the sample.

16%CSMA20%-4FT-PVAn%	Instantaneous modulus (kPa) (1%/s)	Equilibrium modulus (kPa) (5%/s)	Stress at failure (kPa)	Strain at failure (%)
16%CSMA20%: Control	340± 26	363± 71	210± 40	38± 7
4FT-PVA 5%	45-60	?	High	High
16%CSMA20%-FT-PVA0.3%	459± 99	433± 41	211± 72	30± 6
16%CSMA20%-FT-PVA0.5%	461± 102	584± 50	298± 95	44± 3
16%CSMA20%-FT-PVA1%	730± 178	NA	159± 23	21± 5

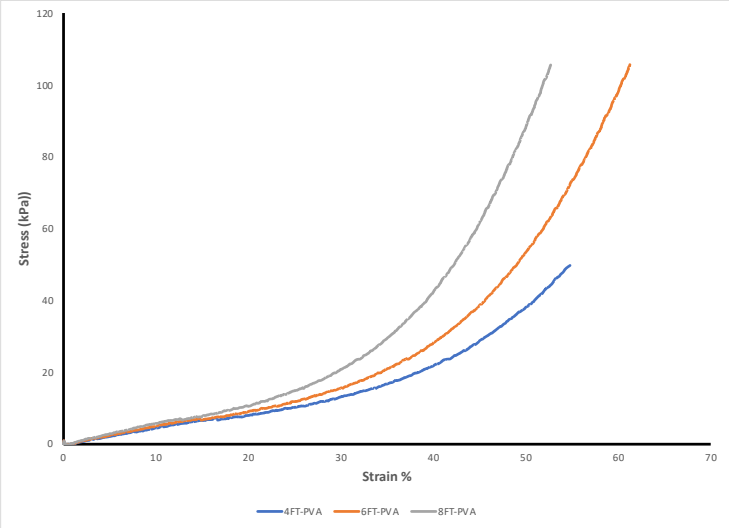

Figure 34: Stress vs. strain curve of nFT-PVA 5%. n indicates the number of freeze-thaw cycles. Measured with 1N load cell at rate 16%/s .4FT-PVA (Blue), 6FT-PVA (Orange) and 8FT-PVA (grey).

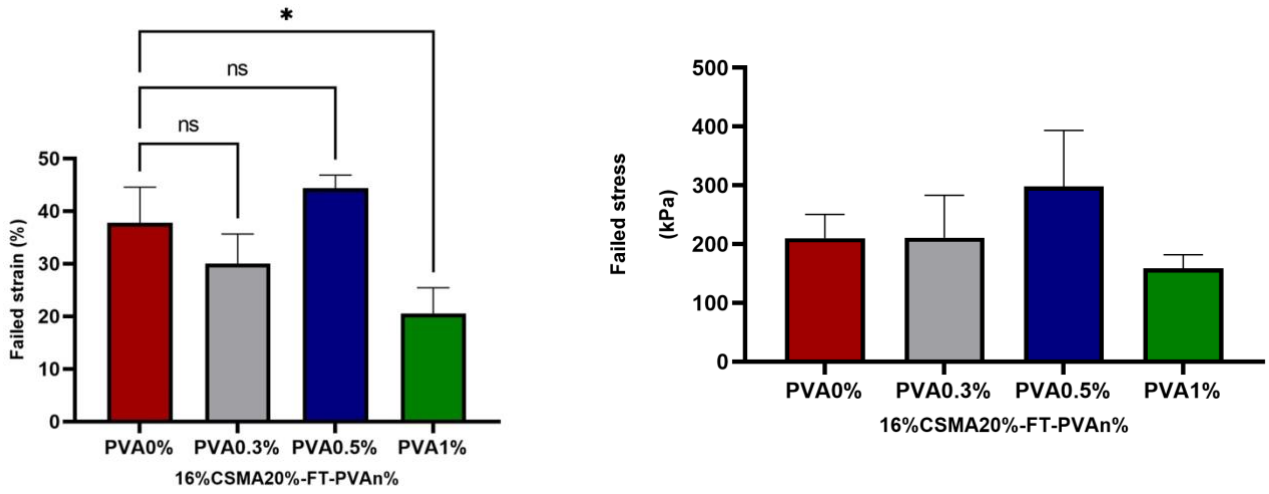

Figure 35: Failed stress (left) and strain (right) of the hydrogels with PVA concentration 0% to 1% at 1%/s loading. Significance is indicated in the figures between the control sample (PVA0%) and hydrogels containing FT-PVA (0.05 < p > 0.01, ** 0.01 < p > 0.001, *** p <= 0.0001). ns indicates that there is no difference between data sets.*

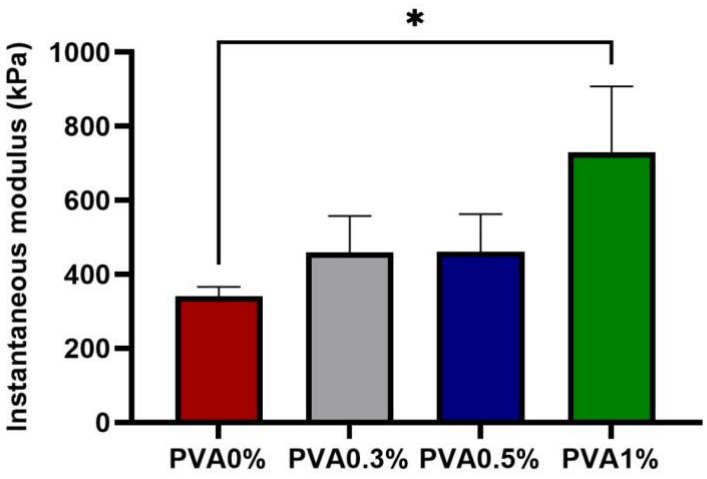

Figure 36: Instantaneous modulus of the hydrogels in the region of 0-5% strain. Significance is indicated in the figures between the control sample (PVA0%) and hydrogels containing FT-PVA (0.05 < p > 0.01). Error bars represent SD with an n of 3.*

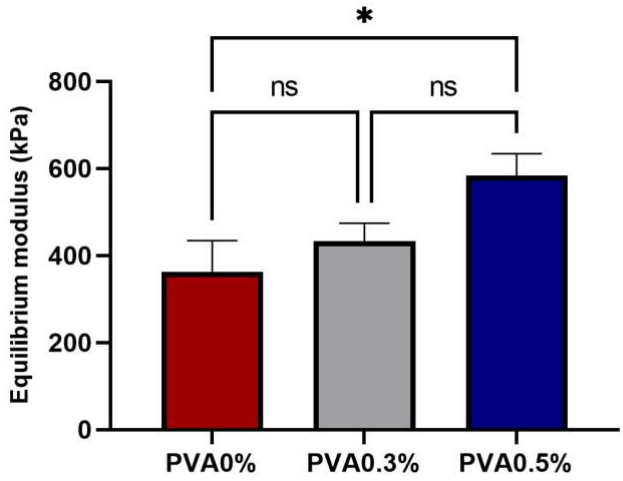

Figure 37: Equilibrium modulus of the hydrogels with PVA concentration 0% to 0.5% at 5%/s loading. The hydrogel containing 1% PVA was brittle and not able to be measured. Significance is indicated in the figures between the control sample (PVA0%) and hydrogels containing FT-PVA (0.05 < p > 0.01, ** 0.01 < p > 0.001, *** p <= 0.0001).*

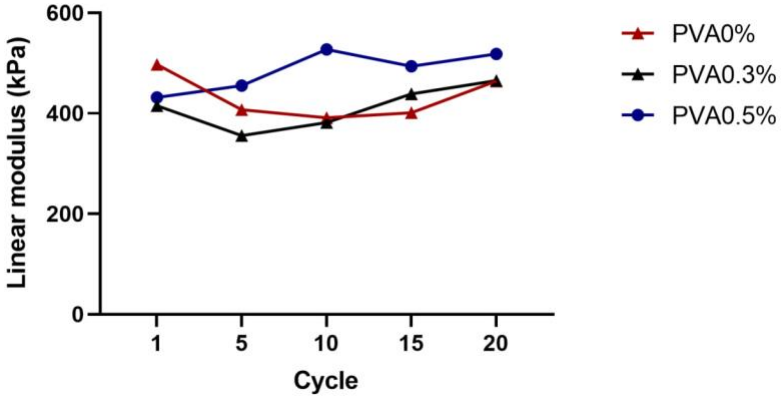

Figure 38: Representative linear modulus (2-8% strain) of 16%CSMA20% (red), 16%CSMA20%-PVA0.3% (black) and 16%CSMA20%-PVA0.5% (blue) throughout 20 compression cycles at 1%/s loading.

3.4 Conclusions and recommendations

The CS/FT-PVA-based hydrogels were obtained by combining chemical and physical cross-linking methods. The methacrylate chondroitin sulfate (CS) was chemically crosslinked using UV light in various cross-linking conditions, prepolymer concentration and degree of Methacrylation to optimize the mechanical properties of the hydrogel. Poly(vinyl alcohol) (PVA) 5% w/v was subjected to freeze-thaw (FT) cycles to allow the formation of physical networks and micronized to be incorporated into the hydrogel to improve the mechanical properties of the chondroitin sulphate hydrogel. FT-PVA incorporated in methacrylate chondroitin sulphate in this method is a material that can be injectable and used potentially in the presence of cells and crosslinked in place using UV or a thermo-initiator. Basically, the incorporation of PVA into a hydrogel created a stiff hydrogel within an elastic one and the presence of just a small amount of this stuff (1% w/v) showed a high increase of the modulus that becomes comparable to that of articular cartilage. The systems also showed a low sol-content with low cytotoxicity and a high-water content suitable for medical applications. Our results highlight the effect of the FT-PVA component on the mechanical performance of hydrogels. The cyclic compressive moduli of all hydrogels under 20 cycles showed a promising characteristic with no damage up to 20% strain. Further work is required to optimize the mechanical properties and evaluate the performance of the hydrogels incorporated with the cells. Cell Corporation for Regeneration: This involves optimizing the hydrogel composition and structure to create an optimal microenvironment for cell growth and differentiation. This includes enhancing mechanical properties, increasing cell viability, and improving integration with the surrounding tissue.

The future perspectives of injectable hydrogels made of natural polymers such as Chondroitin Sulfate (CS) and their combination with freeze-thawed Polyvinyl Alcohol (FT-PVA) in the treatment of articular cartilage are as follows:

a. Controlled Drug Delivery: Incorporating bioactive molecules, growth factors, or anti-inflammatory drugs enables sustained and localized delivery of therapeutic agents. Future developments aim to fine-tune release kinetics, improve drug loading efficiency, and tailor delivery profiles to specific stages of cartilage repair.
b. Bioactive Modification: Introducing specific functional groups or motifs allows precise control over hydrogel properties and interactions with cells and tissues.
c. Bioactive modifications enhance cell adhesion, promote extracellular matrix production, and influence cellular behaviour, leading to improved cartilage healing and integration.

References

1. Bonilla, L.; Espina, M.; Severino, P.; Cano, A.; Ettcheto, M.; Camins, A.; García, M.L.; Souto, E.B.; Sánchez-López, E. Lipid Nanoparticles for the Posterior Eye Segment. *Pharmaceutics* 2022, *14*.
2. Gene vision Https://Gene.Vision/Knowledge-Base/Retina/.
3. Ramírez, J.M.; Ramírez, A.I.; Salazar, J.J.; de Hoz, R.; Trivio, A. Changes of Astrocytes in Retinal Ageing and Age-Related Macular Degeneration. *Exp Eye Res* **2001**, *73*, 601–615, doi:10.1006/EXER.2001.1061.
4. Bourne, R.R.A.; Flaxman, S.R.; Braithwaite, T.; Cicinelli, M. v.; Das, A.; Jonas, J.B.; Keeffe, J.; Kempen, J.; Leasher, J.; Limburg, H.; et al. Magnitude, Temporal Trends, and Projections of the Global Prevalence of Blindness and Distance and near Vision Impairment: A Systematic Review and Meta-Analysis. *Lancet Glob Health* **2017**, *5*, e888–e897, doi:10.1016/S2214-109X(17)30293-0.
5. Aggarwal, D.; Kaur, I.P. Improved Pharmacodynamics of Timolol Maleate from a Mucoadhesive Niosomal Ophthalmic Drug Delivery System. *Int J Pharm* **2005**, *290*, 155–159, doi:10.1016/J.IJPHARM.2004.10.026.
6. Tsai, C.H.; Wang, P.Y.; Lin, I.C.; Huang, H.; Liu, G.S.; Tseng, C.L. Ocular Drug Delivery: Role of Degradable Polymeric Nanocarriers for Ophthalmic Application. *Int J Mol Sci* 2018, *19*.
7. de Matteis, V.; Rizzello, L. Noble Metals and Soft Bio-Inspired Nanoparticles in Retinal Diseases Treatment: A Perspective. *Cells* 2020, *9*.
8. Rajput, A.; Sharma, P.; Sharma, R.; Thakur, S. *Novel Topical Drug Delivery Systems in Ophthalmic Applications*;

9. Gan, L.; Wang, J.; Jiang, M.; Bartlett, H.; Ouyang, D.; Eperjesi, F.; Liu, J.; Gan, Y. Recent Advances in Topical Ophthalmic Drug Delivery with Lipid-Based Nanocarriers. *Drug Discov Today* 2013, *18*, 290–297.

10. du Toit, L.C.; Pillay, V.; Choonara, Y.E.; Govender, T.; Carmichael, T. Ocular Drug Delivery - A Look towards Nanobioadhesives. *Expert Opin Drug Deliv* 2011, *8*, 71–94.

11. Sahoo, S.K.; Dilnawaz, F.; Krishnakumar, S. Nanotechnology in Ocular Drug Delivery. *Drug Discov Today* **2008**, *13*, 144–151, doi:10.1016/J.DRUDIS.2007.10.021.

12. Kanásová, M.; Nesměrák, K. Systematic Review of Liposomes' Characterization Methods. *Monatsh Chem* 2017, *148*, 1581–1593.

13. Kumar, A.; Badde, S.; Kamble, R.; Pokharkar, V.B. *DEVELOPMENT AND CHARACTERIZATION OF LIPOSOMAL DRUG DELIVERY SYSTEM FOR NIMESULIDE*;

14. Nakhaei, P.; Margiana, R.; Bokov, D.O.; Abdelbasset, W.K.; Jadidi Kouhbanani, M.A.; Varma, R.S.; Marofi, F.; Jarahian, M.; Beheshtkhoo, N. Liposomes: Structure, Biomedical Applications, and Stability Parameters With Emphasis on Cholesterol. *Front Bioeng Biotechnol* 2021, *9*.

15. Honda, M.; Asai, T.; Oku, N.; Araki, Y.; Tanaka, M.; Ebihara, N. Liposomes and Nanotechnology in Drug Development: Focus on Ocular Targets. *Int J Nanomedicine* 2013, *8*, 495–504.

16. Marks, R.; Marks, R. Osteoarthritis and Articular Cartilage: Biomechanics and Novel Treatment Paradigms. *Adv Aging Res* **2014**, *03*, 297–309, doi:10.4236/aar.2014.34039.

17. GUIDE TO SEVERE KNEE ARTHRITIS (TRICOMPARTMENTAL OSTEOARTHRITIS) Https://Springloadedtechnology.Com/Guide-to-Severe-Knee-Osteoarthritis/.

18. Medvedeva, E. v.; Grebenik, E.A.; Gornostaeva, S.N.; Telpuhov, V.I.; Lychagin, A. v.; Timashev, P.S.; Chagin, A.S. Repair of Damaged Articular Cartilage: Current Approaches and Future Directions. *Int J Mol Sci* 2018, *19*.

19. van Onsem, S.; Verstraete, M.; van Eenoo, W.; van der Straeten, C.; Victor, J. Are TKA Kinematics During Closed Kinetic Chain Exercises Associated with Patient-Reported Outcomes? A Preliminary Analysis. *Clin Orthop Relat Res* **2020**, *478*, 255–263, doi:10.1097/CORR.0000000000000991.

20. Sophia Fox, A.J.; Bedi, A.; Rodeo, S.A. The Basic Science of Articular Cartilage: Structure, Composition, and Function. *Sports Health* **2009**, *1*, 461–468, doi:10.1177/1941738109350438.

21. Little, C.J.; Bawolin, N.K.; Chen, X. Mechanical Properties of Natural Cartilage and Tissue-Engineered Constructs. *Tissue Eng Part B Rev* **2011**, *17*, 213–227, doi:10.1089/ten.teb.2010.0572.

22. Mow, V.C.; Guo, X.E. Mechano-Electrochemical Properties of Articular Cartilage: Their Inhomogeneities and Anisotropies. *Annu Rev Biomed Eng* 2002, *4*, 175–209.

23. Atoufi, Z.; Kamrava, S.K.; Davachi, S.M.; Hassanabadi, M.; Saeedi Garakani, S.; Alizadeh, R.; Farhadi, M.; Tavakol, S.; Bagher, Z.; Hashemi Motlagh, G. Injectable PNIPAM/Hyaluronic Acid Hydrogels Containing Multipurpose Modified Particles for Cartilage Tissue Engineering: Synthesis, Characterization, Drug Release and Cell Culture Study. *Int J Biol Macromol* **2019**, *139*, 1168–1181, doi:10.1016/J.IJBIOMAC.2019.08.101.

24. Ngadimin, K.D.; Stokes, A.; Gentile, P.; Ferreira, A.M. Biomimetic Hydrogels Designed for Cartilage Tissue Engineering. *Biomater Sci* 2021, *9*, 4246–4259.

25. Deng, Z.; Jin, J.; Wang, S.; Qi, F.; Chen, X.; Liu, C.; Li, Y.; Ma, Y.; Lyu, F.; Zheng, Q. Narrative Review of the Choices of Stem Cell Sources and Hydrogels for Cartilage Tissue Engineering. *Ann Transl Med* **2020**, *8*, 1598–1598, doi:10.21037/atm-20-2342.

26. Nikolova, M.P.; Chavali, M.S. Recent Advances in Biomaterials for 3D Scaffolds: A Review. *Bioact Mater* **2019**, *4*, 271–292, doi:10.1016/J.BIOACTMAT.2019.10.005.

27. Figueroa-Pizano, M.D.; Vélaz, I.; Martínez-Barbosa, M.E. A Freeze-Thawing Method to Prepare Chitosan-Poly(Vinyl Alcohol) Hydrogels Without Crosslinking Agents and Diflunisal Release Studies. *JoVE* **2020**.

28. Kim, H.D.; Lee, Y.; Kim, Y.; Hwang, Y.; Hwang, N.S. Biomimetically Reinforced Polyvinyl Alcohol-Based Hybrid Scaffolds for Cartilage Tissue Engineering. *Polymers (Basel)* **2017**, *9*, doi:10.3390/polym9120655.

29. Boia, R.; Ruzafa, N.; Aires, I.D.; Pereiro, X.; Ambrósio, A.F.; Vecino, E.; Santiago, A.R. Neuroprotective Strategies for Retinal Ganglion Cell Degeneration: Current Status and Challenges Ahead. *Int J Mol Sci* 2020, *21*.

30. Parisi, V.; Centofanti, M.; Ziccardi, L.; Tanga, L.; Michelessi, M.; Roberti, G.; Manni, G. Treatment with Citicoline Eye Drops Enhances Retinal Function and Neural Conduction along the Visual Pathways in Open Angle Glaucoma. *Graefe's Archive for Clinical and Experimental Ophthalmology* **2015**, *253*, 1327–1340, doi:10.1007/s00417-015-3044-9.

31. You, M.; Rong, R.; Zeng, Z.; Xia, X.; Ji, D. Transneuronal Degeneration in the Brain During Glaucoma. *Front Aging Neurosci* 2021, *13*.

32. Gandolfi, S.; Marchini, G.; Caporossi, A.; Scuderi, G.; Tomasso, L.; Brunoro, A. Cytidine 5′-Diphosphocholine (Citicoline): Evidence for a Neuroprotective Role in Glaucoma. *Nutrients* **2020**, *12*, doi:10.3390/nu12030793.

33. Parisi, V.; Oddone, F.; Ziccardi, L.; Roberti, G.; Coppola, G.; Manni, G. Citicoline and Retinal Ganglion Cells: Effects on Morphology and Function. *Curr Neuropharmacol* **2017**, *16*, 919–932, doi:10.2174/1570159x15666170703111729.

34. Parisi, V. Electrophysiological Assessment of Glaucomatous Visual Dysfunction during Treatment with Cytidine-5′-Diphosphocholine (Citicoline): A Study of 8 Years of Follow-Up. *Documenta Ophthalmologica* **2005**, *110*, 91–102, doi:10.1007/s10633-005-7348-7.

35. SecadesRevNeurol2016.

36. Gandolfi, S.; Marchini, G.; Caporossi, A.; Scuderi, G.; Tomasso, L.; Brunoro, A. Cytidine 5′-Diphosphocholine (Citicoline): Evidence for a Neuroprotective Role in Glaucoma. *Nutrients* **2020**, *12*, doi:10.3390/nu12030793.

37. Liu, J. Interfacing Zwitterionic Liposomes with Inorganic Nanomaterials: Surface Forces, Membrane Integrity, and Applications. *Langmuir* **2016**, *32*, 4393–4404, doi:10.1021/acs.langmuir.6b00493.

38. Hathout, R.M.; Mansour, S.; Mortada, N.D.; Guinedi, A.S. *Liposomes as an Ocular Delivery System for Acetazolamide: In Vitro and In Vivo Studies*;

39. Baranowski, P.; Karolewicz, B.; Gajda, M.; Pluta, J. Ophthalmic Drug Dosage Forms: Characterisation and Research Methods. *The Scientific World Journal* 2014, *2014*.

40. Monteiro, N.; Martins, A.; Reis, R.L.; Neves, N.M. Liposomes in Tissue Engineering and Regenerative Medicine. *J R Soc Interface* 2014, *11*.

41. Garrigue, J.S.; Amrane, M.; Faure, M.O.; Holopainen, J.M.; Tong, L. Relevance of Lipid-Based Products in the Management of Dry Eye Disease. *Journal of Ocular Pharmacology and Therapeutics* 2017, *33*, 647–661.

42. Vemuri, S.; Rhodes, C.T. *Preparation and Characterization of Liposomes as Therapeutic Delivery Systems: A Review*; 1995; Vol. 70;.

43. Agarwal, R.; Iezhitsa, I.; Agarwal, P.; Abdul Nasir, N.A.; Razali, N.; Alyautdin, R.; Ismail, N.M. Liposomes in Topical Ophthalmic Drug Delivery: An Update. *Drug Deliv* 2016, *23*, 1075–1091.

44. Jaafar-Maalej, C.; Diab, R.; Andrieu, V.; Elaissari, A.; Fessi, H. Ethanol Injection Method for Hydrophilic and Lipophilic Drug-Loaded Liposome Preparation. *J Liposome Res* **2010**, *20*, 228–243, doi:10.3109/08982100903347923.

45. Conant, R.; Schauss, A.G. *Therapeutic Applications of Citicoline for Stroke and Cognitive Dysfunction in the Elderly: A Review of the Literature*; 2004; Vol. 9;.

46. Secades, J.J. *Diagnosis of Mild Cognitive Impairment View Project Updating the Evidence for Citicoline View Project*; 2006;

47. Adibhatla, R.M.; Hatcher, J.F.; Dempsey, R.J. Citicoline: Neuroprotective Mechanisms in Cerebral Ischemia. *J Neurochem* 2002, *80*, 12–23.

48. Frézard, F.; Silva-Barcellos, N.M.; dos Santos, R.A.S. A Novel Approach Based on Nanotechnology for Investigating the Chronic Actions of Short-Lived Peptides in Specific Sites of the Brain. *Regul Pept* **2007**, *138*, 59–65, doi:10.1016/J.REGPEP.2006.11.021.

49. Çağdaş, M.; Sezer, A.D.; Bucak, S. Liposomes as Potential Drug Carrier Systems for Drug Delivery. In *Application of Nanotechnology in Drug Delivery*; InTech, 2014.

50. Popovska, O.; Klopcevska, J.; Kavrakovski, Z.; Simonovska, J.; Rafajlovska, V. *An Overview: Methods for Preparation and Characterization of Liposomes as Drug*

Delivery Systems SOURDOMICS-Sourdough Biotechnology Network towards Novel, Healthier and Sustainable Food and Bioprocesses"-CA 18101, Dissemination Board Member. View Project Toksicni Hemikalii View Project An Overview: Methods for Preparation and Characterization of Liposomes as Drug Delivery Systems; 2013; Vol. 3;.

51. Costa, A.P.; Xu, X.; Burgess, D.J. Freeze-Anneal-Thaw Cycling of Unilamellar Liposomes: Effect on Encapsulation Efficiency. *Pharm Res* **2014**, *31*, 97–103, doi:10.1007/s11095-013-1135-z.

52. Traõè Kia Á Dror, M.; Warschawski, E.; Recouvreur, M.; Cartaud, J.; Devaux, P.F. *Formation of Unilamellar Vesicles by Repetitive Freeze-Thaw Cycles: Characterization by Electron Microscopy and 31 P-Nuclear Magnetic Resonance*;

53. Bertsch, P.; Bergfreund, J.; Windhab, E.J.; Fischer, P. Physiological Fluid Interfaces: Functional Microenvironments, Drug Delivery Targets, and First Line of Defense. *Acta Biomater* 2021, *130*, 32–53.

54. Bulbake, U.; Doppalapudi, S.; Kommineni, N.; Khan, W. Liposomal Formulations in Clinical Use: An Updated Review. *Pharmaceutics* 2017, *9*.

55. Holsæter, A.M.; Wizgird, K.; Karlsen, I.; Hemmingsen, J.F.; Brandl, M.; Škalko-Basnet, N. How Docetaxel Entrapment, Vesicle Size, Zeta Potential and Stability Change with Liposome Composition–A Formulation Screening Study. *European Journal of Pharmaceutical Sciences* **2022**, *177*, 106267, doi:10.1016/J.EJPS.2022.106267.

56. Eloy, J.O.; Claro de Souza, M.; Petrilli, R.; Barcellos, J.P.A.; Lee, R.J.; Marchetti, J.M. Liposomes as Carriers of Hydrophilic Small Molecule Drugs: Strategies to Enhance Encapsulation and Delivery. *Colloids Surf B Biointerfaces* **2014**, *123*, 345–363, doi:10.1016/J.COLSURFB.2014.09.029.

57. Subczynski, W.K.; Pasenkiewicz-Gierula, M.; Widomska, J.; Mainali, L.; Raguz, M. High Cholesterol/Low Cholesterol: Effects in Biological Membranes: A Review. *Cell Biochem Biophys* **2017**, *75*, 369–385, doi:10.1007/s12013-017-0792-7.

58. Nogueira, E.; Gomes, A.C.; Preto, A.; Cavaco-Paulo, A. Design of Liposomal Formulations for Cell Targeting. *Colloids Surf B Biointerfaces* **2015**, *136*, 514–526, doi:10.1016/J.COLSURFB.2015.09.034.

59. Chibowski, E.; Szcześ, A. Zeta Potential and Surface Charge of DPPC and DOPC Liposomes in the Presence of PLC Enzyme. *Adsorption* **2016**, *22*, 755–765, doi:10.1007/s10450-016-9767-z.

60. Verma, D.D.; Verma, S.; Blume, G.; Fahr, A. Particle Size of Liposomes Influences Dermal Delivery of Substances into Skin. *Int J Pharm* **2003**, *258*, 141–151, doi:10.1016/S0378-5173(03)00183-2.

61. Halevas, E.G.; Avgoulas, D.I.; Katsipis, G.; Pantazaki, A.A. Flavonoid-Liposomes Formulations: Physico-Chemical Characteristics, Biological Activities and Therapeutic Applications. *European Journal of Medicinal Chemistry Reports* **2022**, *5*, 100059, doi:10.1016/J.EJMCR.2022.100059.

62. Bonechi, C.; Tamasi, G.; Donati, A.; Leone, G.; Consumi, M.; Cangeloni, L.; Volpi, V.; Magnani, A.; Cappelli, A.; Rossi, C. Physicochemical Characterization of Hyaluronic Acid and Chitosan Liposome Coatings. *Applied Sciences (Switzerland)* **2021**, *11*, doi:10.3390/app112412071.

63. Bonechi, C.; Donati, A.; Tamasi, G.; Pardini, A.; Rostom, H.; Leone, G.; Lamponi, S.; Consumi, M.; Magnani, A.; Rossi, C. Chemical Characterization of Liposomes Containing Nutraceutical Compounds: Tyrosol, Hydroxytyrosol and Oleuropein. *Biophys Chem* **2019**, *246*, 25–34, doi:10.1016/J.BPC.2019.01.002.

64. Sadžak, A.; Mravljak, J.; Maltar-Strmečki, N.; Arsov, Z.; Baranović, G.; Erceg, I.; Kriechbaum, M.; Strasser, V.; Přibyl, J.; Šegota, S. *The Structural Integrity of the Model Lipid Membrane during Induced Lipid Peroxidation: The Role of Flavonols in the Inhibition of Lipid Peroxidation*;

65. Dash, M.; Chiellini, F.; Ottenbrite, R.M.; Chiellini, E. Chitosan—A Versatile Semi-Synthetic Polymer in Biomedical Applications. *Prog Polym Sci* **2011**, *36*, 981–1014, doi:10.1016/J.PROGPOLYMSCI.2011.02.001.

66. Ullah, F.; Othman, M.B.H.; Javed, F.; Ahmad, Z.; Akil, H.M. Classification, Processing and Application of Hydrogels: A Review. *Materials Science and Engineering: C* **2015**, *57*, 414–433, doi:10.1016/J.MSEC.2015.07.053.

67. Reddy, N.; Reddy, R.; Jiang, Q. Crosslinking Biopolymers for Biomedical Applications. *Trends Biotechnol* 2015, *33*, 362–369.

68. Yang, J.A.; Yeom, J.; Hwang, B.W.; Hoffman, A.S.; Hahn, S.K. In Situ-Forming Injectable Hydrogels for Regenerative Medicine. *Prog Polym Sci* **2014**, *39*, 1973–1986, doi:10.1016/J.PROGPOLYMSCI.2014.07.006.

69. Spiller, K.L.; Maher, S.A.; Lowman, A.M. Hydrogels for the Repair of Articular Cartilage Defects. *Tissue Eng Part B Rev* **2011**, *17*, 281–299, doi:10.1089/ten.teb.2011.0077.

70. Ahmed, E.M. Hydrogel: Preparation, Characterization, and Applications: A Review. *J Adv Res* **2015**, *6*, 105–121, doi:10.1016/J.JARE.2013.07.006.

71. Jelvehgari, M.; Lotfipour, F.; Alami-Milani, M.; Salatin, S.; Hadavi, A.; Jelvehgari, M. *Freeze-Thaw-Induced Cross-Linked PVA/Chitosan for Oxytetracycline-Loaded Wound Dressing: The Experimental Design and Optimization*; 2019; Vol. 14;.

72. Louka, D.A.; Holwell, N.; Thomas, B.H.; Chen, F.; Amsden, B.G. Highly Bioactive SDF-1α Delivery from Low-Melting-Point, Biodegradable Polymer Microspheres. *ACS Biomater Sci Eng* **2018**, *4*, 3747–3758, doi:10.1021/acsbiomaterials.7b00403.

73. Sukarto, A.; Amsden, B.G. Low Melting Point Amphiphilic Microspheres for Delivery of Bone Morphogenetic Protein-6 and Transforming Growth Factor-B3 in a Hydrogel Matrix. *Journal of Controlled Release* **2012**, *158*, 53–62, doi:10.1016/j.jconrel.2011.10.015.

74. Schuurmans, C.C.L.; Mihajlovic, M.; Hiemstra, C.; Ito, K.; Hennink, W.E.; Vermonden, T. Hyaluronic Acid and Chondroitin Sulfate (Meth)Acrylate-Based Hydrogels for Tissue Engineering: Synthesis, Characteristics and Pre-Clinical Evaluation. *Biomaterials* **2021**, *268*, 120602, doi:10.1016/J.BIOMATERIALS.2020.120602.

Appendix- Supplemental Information

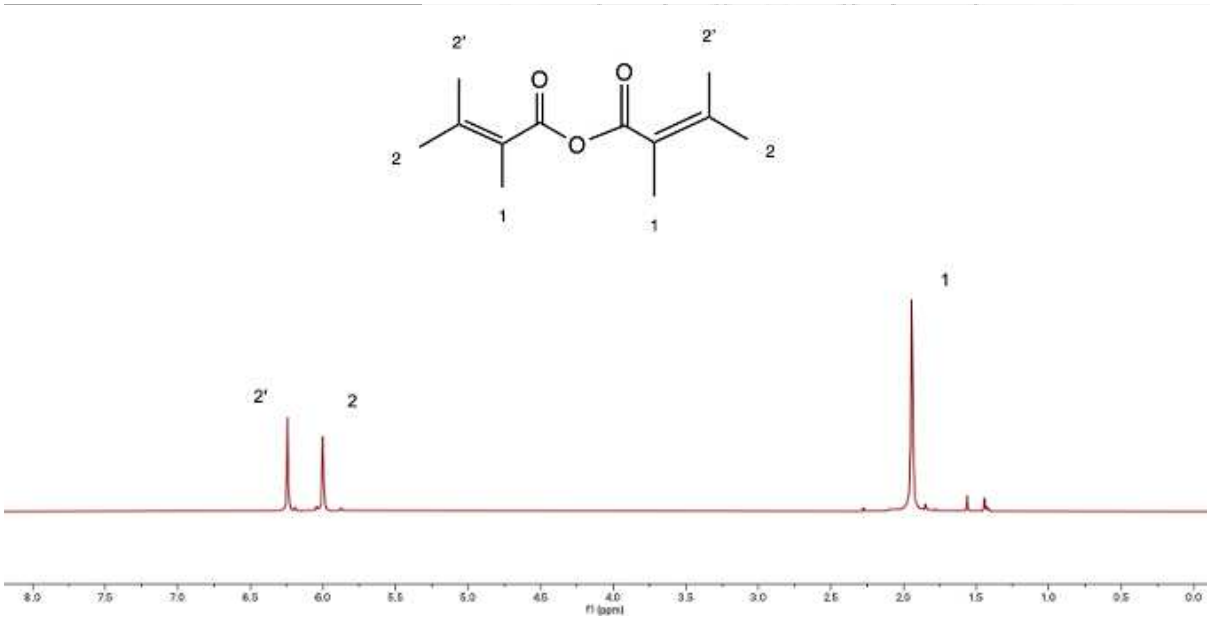

FigureA2- 1: Representative ^{1}H-NMR spectrum (DMSO-d_6, 400 MHz) of the methacrylate anhydride.

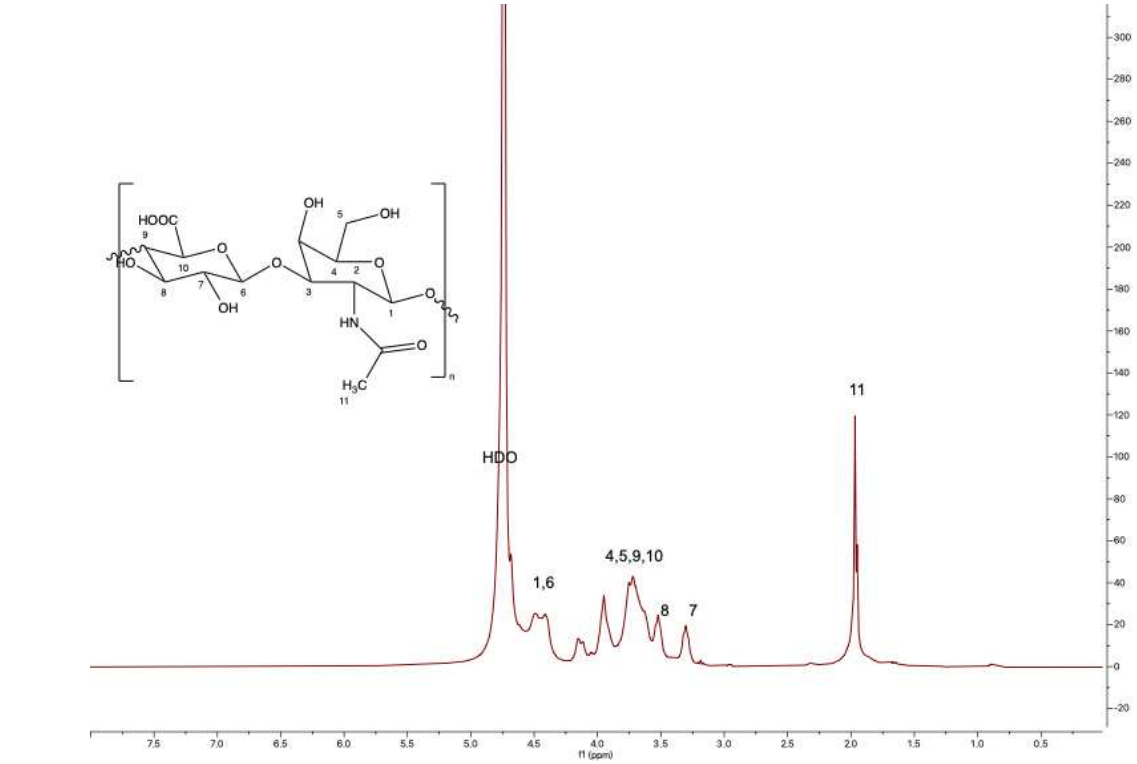

FigureA2- 2: Representative [1]H-NMR spectrum (D_2O, 400 MHz) of the chondroitin sulfate.

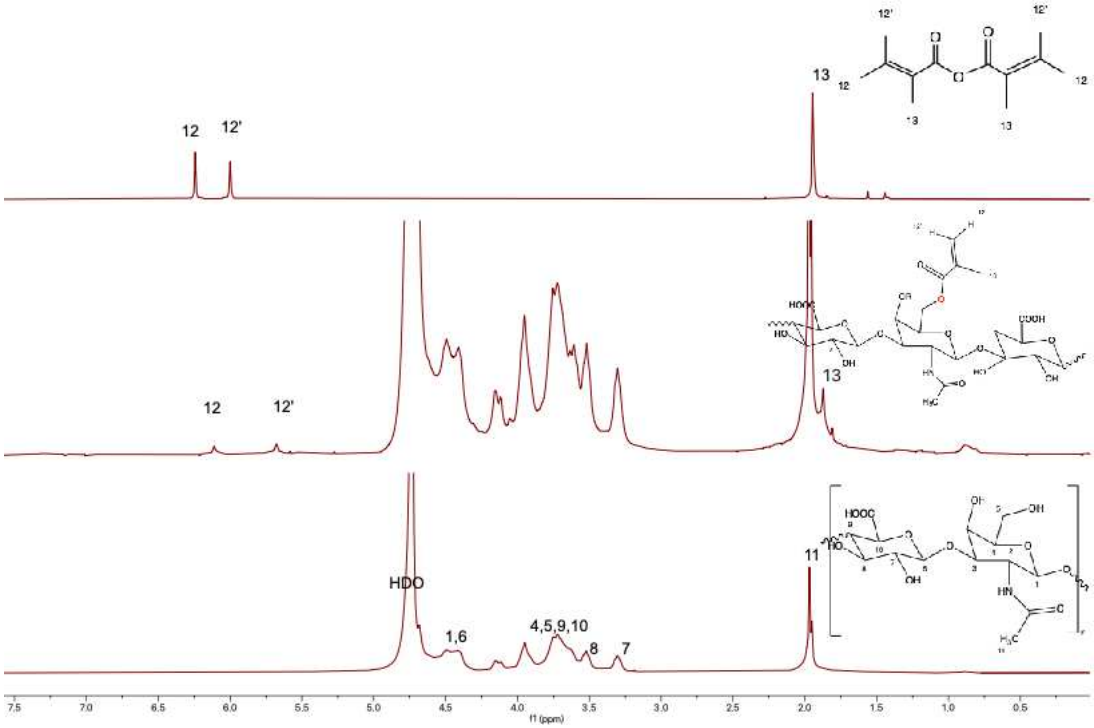

FigureA2- 3: Representative stacked [1]H-NMR spectrum (D2O, 400 MHz) of the methacrylate chondroitin sulfate CS: MAh 1:5 excess molar ratio(bottom), chondroitin sulfate (middle), and methacrylate anhydride(top).

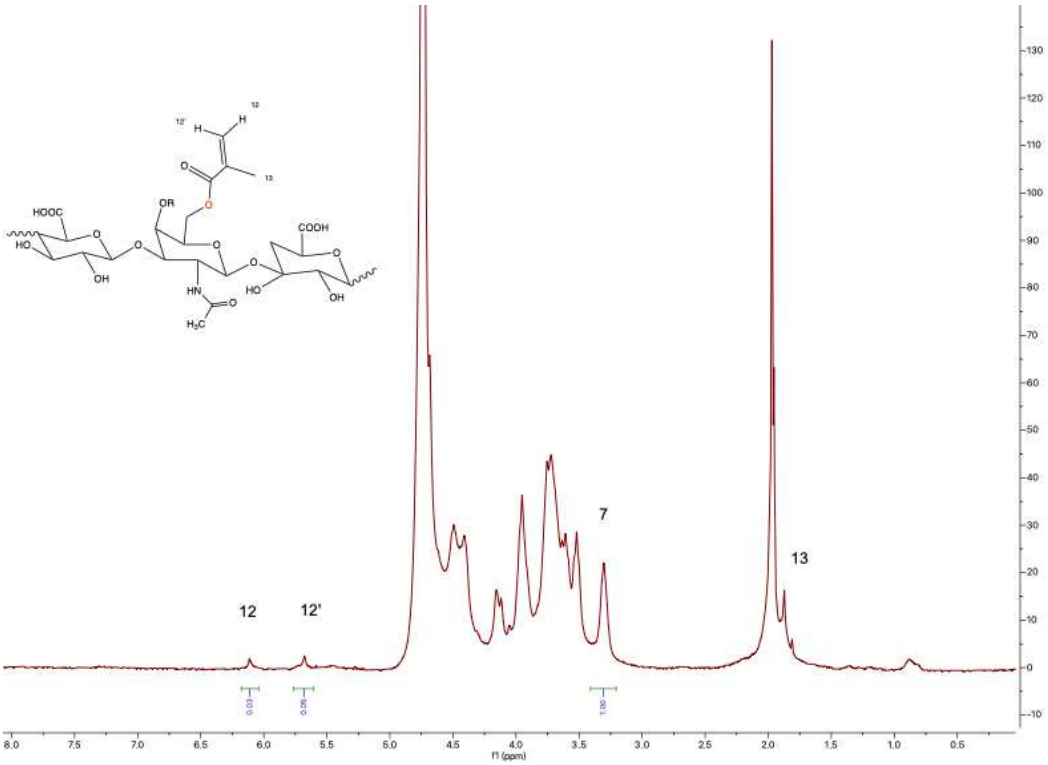

FigureA2- 4: Representative [1]H-NMR spectrum (D_2O, 400 MHz) of the methacrylate chondroitin sulfate CS: MAh 1:5 excess molar ratio.

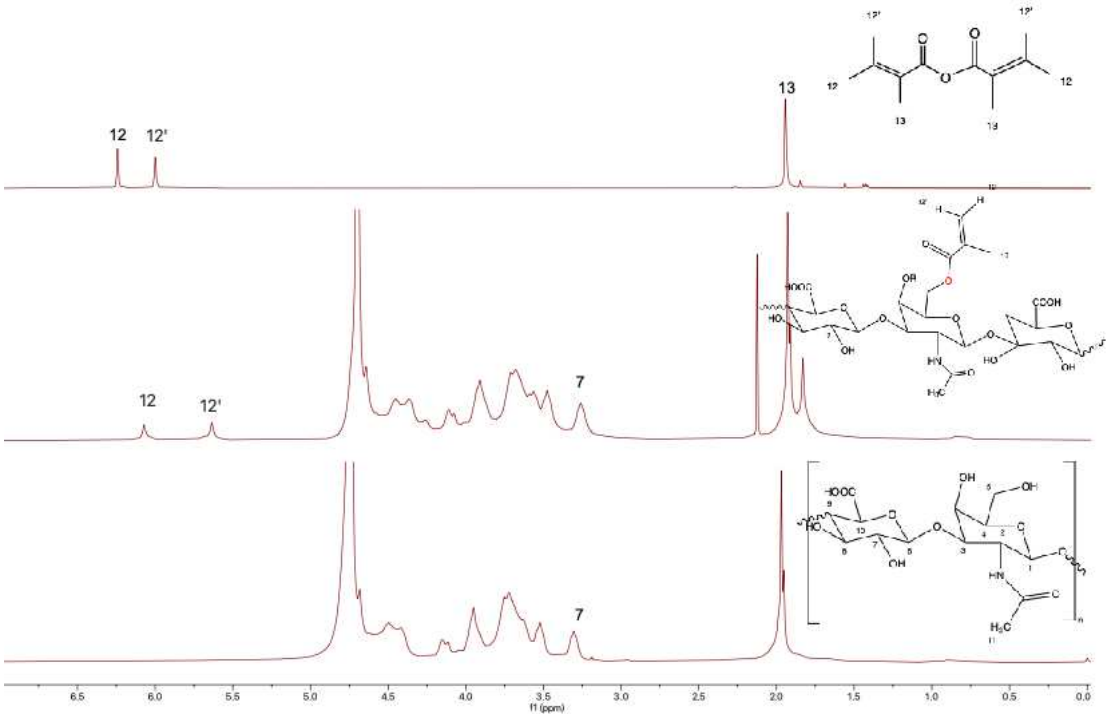

FigureA2- 5: Representative stacked ^{1}H-NMR spectrum (D_2O, 400 MHz) of the methacrylate chondroitin sulfate CS: MAh 1:12 excess molar ratio(bottom), chondroitin sulfate (middle), and methacrylic anhydride(top).

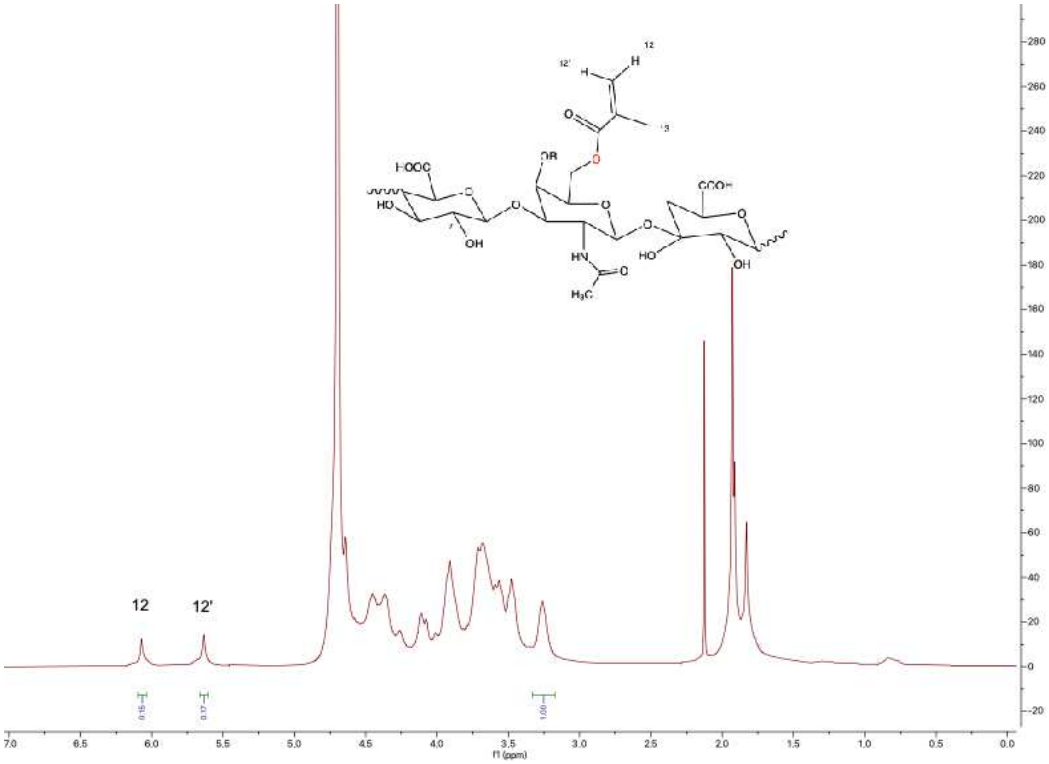

FigureA2- 6: Representative 1H-NMR spectrum (D_2O, 400 MHz) of the methacrylate chondroitin sulfate CS: MAh 1:12 excess molar ratio.

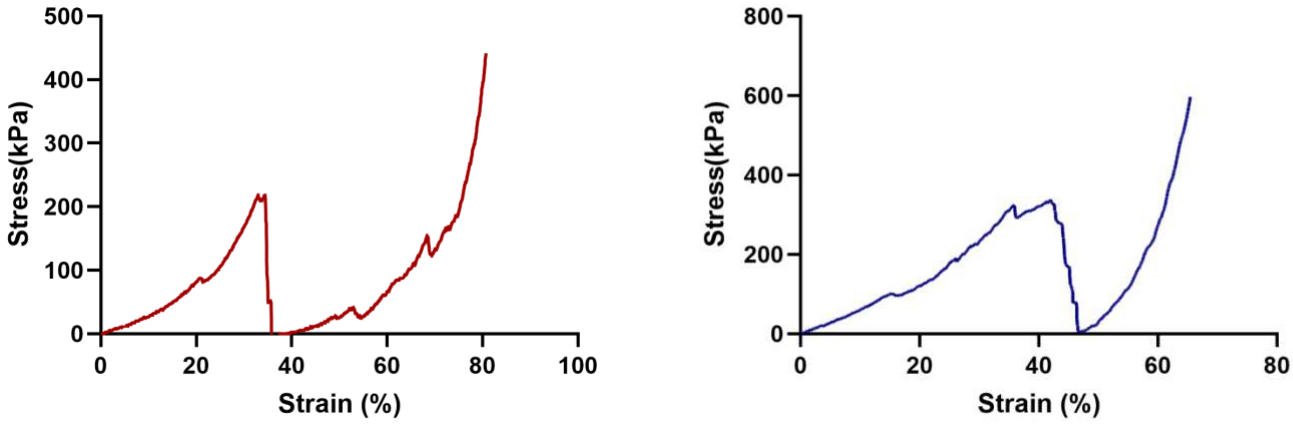

FigureA2- 7: The behaviour of the control sample 16%CSMA20% (left) and 16%CSMA205-PVA0.5% (right) under compressive loading. Samples were compressed at 1%/s loading.

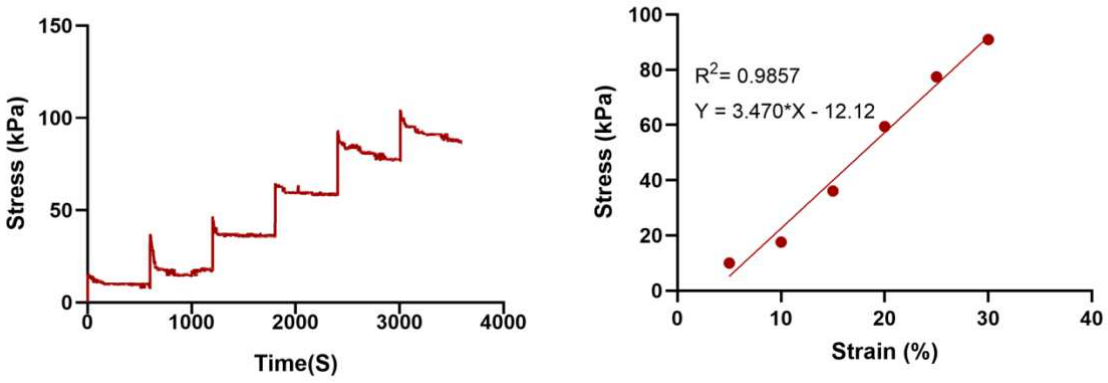

FigureA2- 8: Representative stress relaxation data of 16%CSMA20% (control). Raw data shows a 5% stepwise increase in strain followed by a relaxation period (left). Data analysis of relaxed stress at each step (right) (Rate: 5%/s).

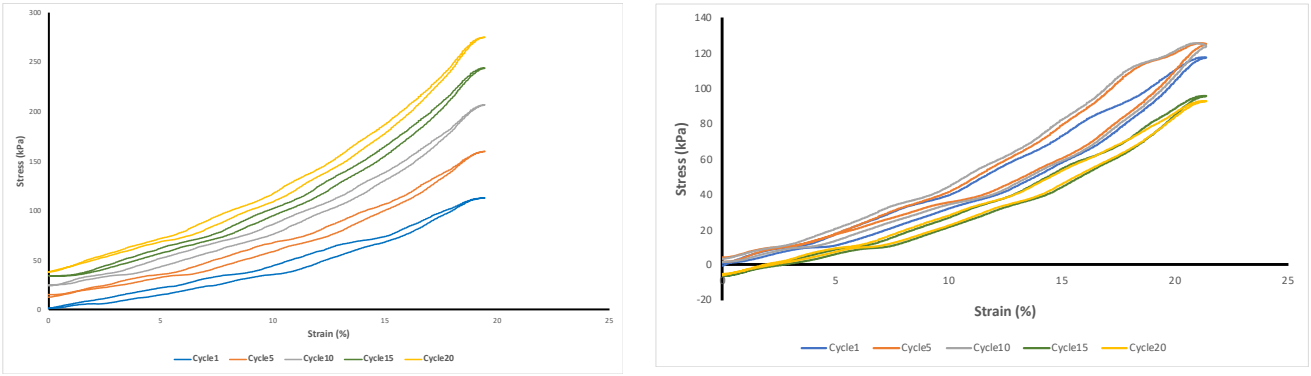

FigureA2- 9: The cyclic compression modulus up to 20% strain throughout 20 compression cycles at 1%/s loading. The control sample (left), CSMA-FT-PVA0.5% (Right).